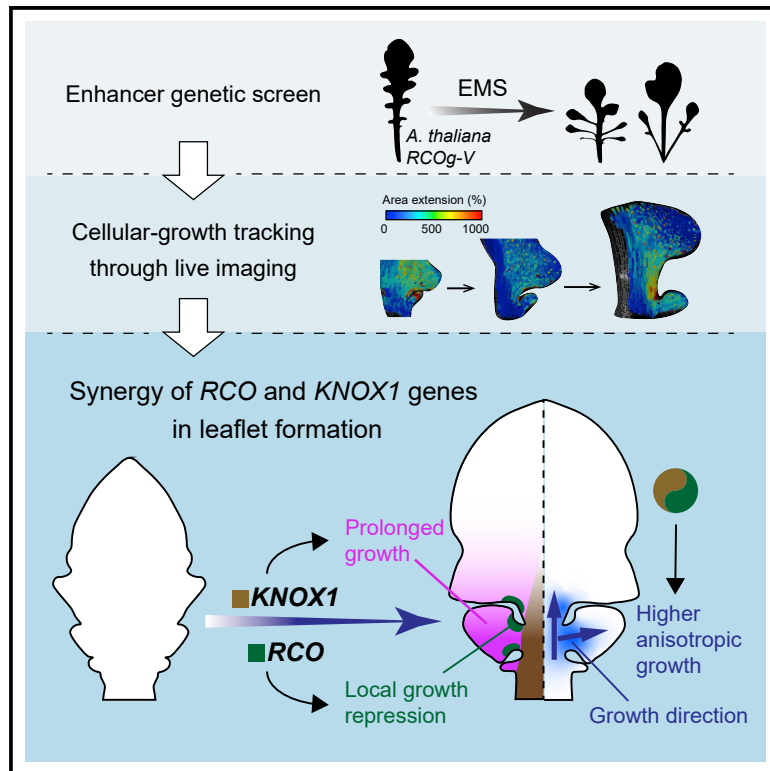


## The cellular basis for synergy between *RCO* and *KNOX1* homeobox genes in leaf shape diversity

### Graphical abstract



### Authors

Yi Wang, Sören Strauss, Shanda Liu, Bjorn Pieper, Rena Lymbouridou, Adam Runions, Miltos Tsiantis

### Correspondence

tsiantis@mpipz.mpg.de

### In brief

Wang et al. use a genetic screen and live imaging to show that synergy of *RCO* and *KNOX1* homeobox genes creates a preferred developmental path for leaflet formation in crucifer plants. The cellular basis for this synergy is a combination of prolonged growth, repressed growth, and anisotropic growth of different cells in the leaf bud.

### Highlights

- An enhancer genetic screen shows synergy of *RCO* and *KNOX1* genes in leaflet formation
- This synergy explains generation of linear shape elements of dissected leaves
- Live imaging of growth unravels the cellular basis of *RCO* and *KNOX1* synergy
- Control of growth anisotropy is a novel facet of *KNOX1* action in leaflet formation



## Article

# The cellular basis for synergy between *RCO* and *KNOX1* homeobox genes in leaf shape diversity

Yi Wang,<sup>1</sup> Sören Strauss,<sup>1</sup> Shanda Liu,<sup>1</sup> Bjorn Pieper,<sup>1</sup> Rena Lymbouridou,<sup>1</sup> Adam Runions,<sup>2</sup> and Miltos Tsiantis<sup>1,3,\*</sup><sup>1</sup>Department of Comparative Development and Genetics, Max Planck Institute for Plant Breeding Research, Carl von Linne Weg 10, 50829 Cologne, Germany<sup>2</sup>Department of Computer Science, University of Calgary, Calgary, AB T2N1N4, Canada<sup>3</sup>Lead contact\*Correspondence: [tsiantis@mpipz.mpg.de](mailto:tsiantis@mpipz.mpg.de)<https://doi.org/10.1016/j.cub.2022.08.020>**SUMMARY**

Leaves of seed plants provide an attractive system to study the development and evolution of form. Leaves show varying degrees of margin complexity ranging from simple, as in *Arabidopsis thaliana*, to fully dissected into leaflets in the closely related species *Cardamine hirsuta*. Leaflet formation requires actions of Class I *KNOTTED1-LIKE HOMEBOX (KNOX1)* and *REDUCED COMPLEXITY (RCO)* homeobox genes, which are expressed in the leaves of *C. hirsuta* but not *A. thaliana*. Evolutionary studies indicate that diversification of *KNOX1* and *RCO* genes was repeatedly associated with increased leaf complexity. However, whether this gene combination represents a developmentally favored avenue for leaflet formation remains unknown, and the cell-level events through which the combined action of these genes drives leaflet formation are also poorly understood. Here we show, through a genetic screen, that when a *C. hirsuta RCO* transgene is expressed in *A. thaliana*, then ectopic *KNOX1* expression in leaves represents a preferred developmental path for leaflet formation. Using time-lapse growth analysis, we demonstrate that *KNOX1* expression in the basal domain of leaves leads to prolonged and anisotropic cell growth. This *KNOX1* action, in synergy with local growth repression by *RCO*, is instrumental in generating rachises and petiolules, the linear geometrical elements, that bear leaflets in complex leaves. Our results show how the combination of cell-level growth analyses and genetics can help us understand how evolutionary modifications in expression of developmentally important genes are translated into diverse leaf shapes.

**INTRODUCTION**

A key challenge in biology is to understand how development influences or biases morphological evolution.<sup>1</sup> One way to address this challenge is to ask whether there are particular genes or combinations of developmental genes whose evolutionary modification creates preferred paths for morphological change. Current evidence suggests that such “hotspot” genes exist, which leads to the question of what intrinsic properties these genes have.<sup>2,3</sup> One idea is that hotspot genes are predisposed to underpin morphological change because their positions in regulatory networks allow them to generate diversity with minimal pleiotropy, thus preventing reduced fitness.<sup>3,4</sup> Less attention has been given to how the cell-level effects of hotspot genes are linked to their capacity to cause diversity in form. Understanding how gene action generates organ shape requires investigating its effects on cellular growth. Plants are attractive systems to study this problem because their development unfolds without cell migration; therefore, the genetic regulation of tissue and organ form can be conceptualized as the cumulative effect of changes in amount, duration, and direction of cellular growth and proliferation.

Leaves of seed plants show a tremendous degree of heritable morphological variation, providing fertile ground for studying interactions of development and evolution. Based on the shapes of

their margins, leaves of seed plants can be broadly classified as simple, with an entire blade, or dissected (also termed compound) into leaflets. Leaflets are borne on the rachis, a central stalk, by smaller stalks called petiolules (Figure 1A). Rachises and petiolules are both narrow, bladeless structures that characterize leaflets and can be considered linear geometrical elements that distinguish simple from dissected leaves.<sup>5</sup> Both simple and dissected leaves can display shallow outgrowths in the form of teeth, serrations, and lobes, leading to further variation in leaf complexity (Figure 1A). *Arabidopsis thaliana* has simple serrated leaves while its relative *Cardamine hirsuta* has dissected leaves (Figure 1A).<sup>6</sup>

Two main genetic pathways have been shown to play a central role in the evolution of leaf complexity in the crucifer lineage, as well as more broadly in seed plants, each defined by a different class of homeobox genes: Class I *KNOTTED-LIKE HOMEBOX (KNOX1)* and HD-ZIP I *REDUCED COMPLEXITY (RCO)* encoding homeodomain transcription factors.<sup>7</sup> *KNOX1* genes are required for meristem maintenance broadly in plant species.<sup>8,9</sup> They are typically not expressed in simple leaves, while their expression in leaves of many seed plant species contributes to the formation of leaflets or lobes.<sup>10–13</sup> There are four *KNOX1* genes in *C. hirsuta* and *A. thaliana*: *SHOOTMERISTEMLESS (STM)*, *BREVIPEDICELLUS/KN1-like in Arabidopsis thaliana1 (BP/KNAT1)*, *KNAT2*, and *KNAT6*. *KNOX1* genes are expressed in *C. hirsuta*



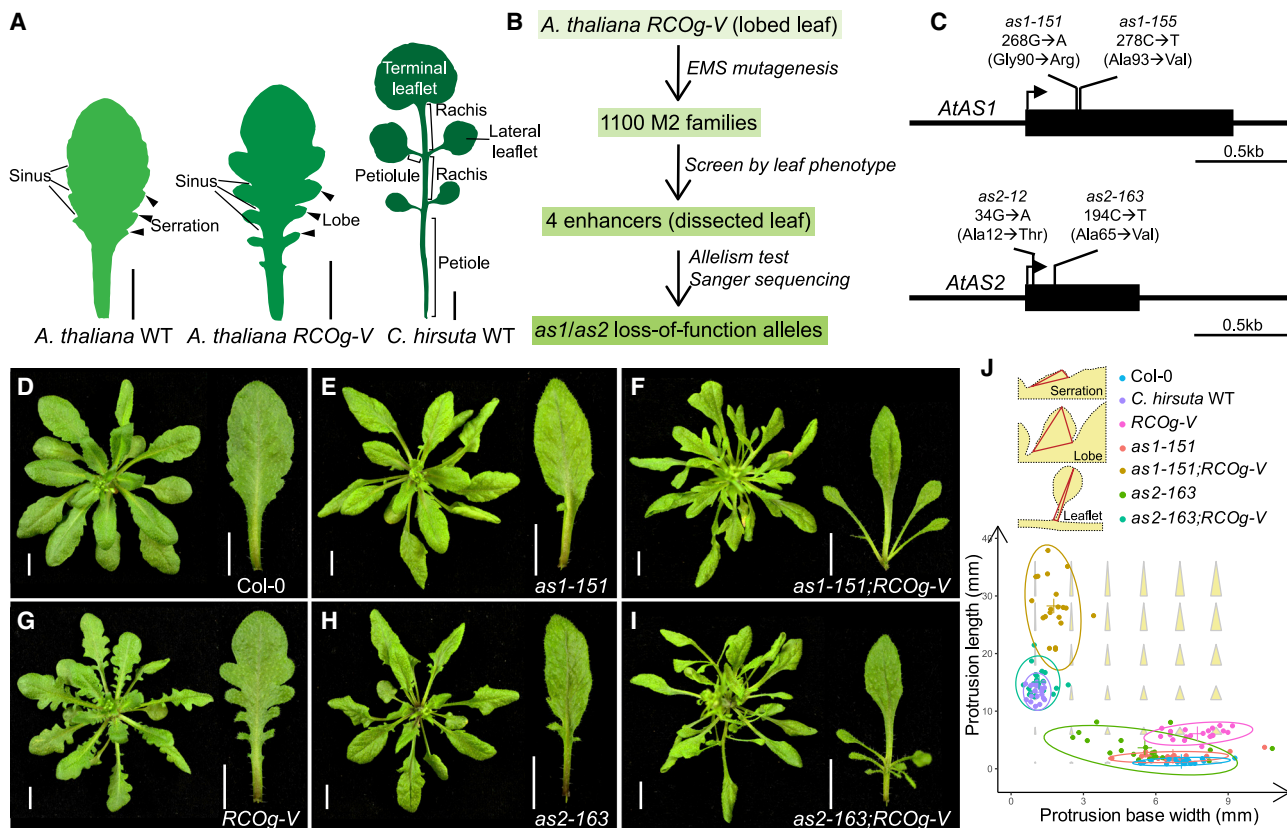


**Figure 1. *as1;RCOg-V* and *as2;RCOg-V* mutants have leaflets instead of lobes**

(A) Silhouettes of a simple serrated leaf from *Arabidopsis thaliana* wild type (WT Col-0), a simple lobed leaf from *A. thaliana RCOg-VENUS* (*RCOg-V*) transgenic plants, and a dissected leaf from *Cardamine hirsuta* wild type, where protrusions (serrations, lobes, and leaflets) and associated anatomical elements are indicated.

(B) Workflow of obtaining *as1/as2* mutant alleles from EMS mutagenesis screen.

(C) Gene structure schematics of *A. thaliana AS1* (*AtAS1*) and *A. thaliana AS2* (*AtAS2*). Exons are drawn as black boxes. Mutants obtained from this screen are labeled with the information of nucleotide/ amino acid substitutions.

(D–I) The rosettes and the 11<sup>th</sup> leaves from Col-0 (D), *as1-151* (E), *as1-151;RCOg-V* (F), *RCOg-V* (G), *as2-163* (H), and *as2-163;RCOg-V* (I) plants.

(J) Analysis of protrusion geometry (length versus base width) in mature rosette leaves of Col-0, *C. hirsuta* wild type, *RCOg-V*, *as1-151*, *as1-151;RCOg-V*, *as2-163*, and *as2-163;RCOg-V* ( $n = 17–20$  per genotype). The cartoon illustrates how each protrusion was approximated as a triangle whose vertices coincide with the protrusion tip and adjoining sinuses. In the plot, the background yellow triangles visualize protrusion shapes as length and base width are varied. The ellipses indicate the 95% confidence regions for each genotype.

Scale bars, 1 cm (A and D–I). See also Figure S1 and Table S1.

but not in *A. thaliana* leaves,<sup>12</sup> and they are required for leaflet development.<sup>12,14</sup> The misexpression of *KNOX1* in *A. thaliana* leaves produces deep lobes.<sup>14–19</sup> *KNOX1* has diverse effects depending on the dose, locality, and context of expression in leaves.<sup>19,20</sup> *KNOX1* expression in leaves is repressed by *ASYMMETRIC LEAVES1/ROUGH SHEATH2/PHANTASTICA* (*ARP*) transcription factors across seed plant species.<sup>12,14,21–24</sup> In *A. thaliana* leaves, *ASYMMETRIC LEAVES1* (*AS1*) directly represses *BP*, *KNAT2*, and *KNAT6* expression (but not *STM*) via forming a complex with *ASYMMETRIC LEAVES2* (*AS2*), a lateral organ boundaries (*LOB*) transcription factor.<sup>21,25–27</sup> Similar to *KNOX1*, *RCO* is expressed in *C. hirsuta* leaves and required for leaflet formation. *RCO* was secondarily lost in the *A. thaliana* lineage, which contributed to leaf simplification.<sup>28</sup> Re-introduction of *ChRCO* into the *A. thaliana* genome as a transgene is sufficient to increase leaf complexity.<sup>28</sup> *RCO* represses growth at the boundaries between leaflets/lobes, and this action is partly mediated

by regulating cytokinin homeostasis.<sup>29</sup> *RCO*-type genes are also required for leaf complexity in *Capsella rubella*,<sup>30</sup> rapeseed,<sup>31</sup> and cotton.<sup>32</sup> Although neither *KNOX1* misexpression nor *ChRCO* transgenic plants in *A. thaliana* generate leaflets, the combination of *KNOX1* and *ChRCO* is sufficient to produce leaflet-like outgrowth and reconstruct dissected leaves in *A. thaliana*.<sup>16</sup>

A number of questions arise from these studies. Is the concurrent expression of *RCO* and *KNOX1* in leaves a preferred developmental path for leaflet formation? What is the precise cell-level effect of *KNOX1* on leaflet formation? While the cumulative evidence supports a role for *KNOX1* conferring a longer duration of cellular growth in leaf development,<sup>16</sup> the various facets of *KNOX1* action and their relevance for leaflet formation require more investigation.

Here, we addressed the issues above by re-introducing *RCO* into the genome of *A. thaliana* and conducting a mutant screen. We aimed to identify, in an unbiased fashion, genes that can

support leaflet formation in *A. thaliana* when *RCO* is present. This screen yielded multiple *as1* and *as2* loss-of-function alleles, in which ectopic *KNOX1* expression in the basal midrib/petiole region of leaf primordia caused leaflet formation when *RCO* is active in leaves. Through time-lapse imaging and growth analysis, we showed that *KNOX1*-dependent, prolonged, and anisotropic cell growth in the basal leaf region, combined with local growth repression by *RCO*, contributes to leaflet formation, particularly to the generation of rachises and petiolules—the linear elements that distinguish simple from dissected leaves. Our results indicate that the combination of *RCO* and *KNOX1* in leaves is a preferred developmental path for leaflet formation in crucifers. They also highlight *KNOX1*-dependent anisotropic growth as an important component of *KNOX1* action in leaflet formation.

## RESULTS

### *as1;RCOg-V* and *as2;RCOg-V* mutants have leaflets instead of lobes

To identify genes that enhance *RCO* to promote leaflet formation in *A. thaliana*, we screened ethylmethanesulfonate mutagenized *RCOg-VENUS* (*RCOg-V*) transgenic lines, which had lobed leaves (Figure 1A).<sup>33</sup> We screened for enhancer mutations that transformed lobes into leaflets, thus resembling wild-type *C. hirsuta* (Oxford strain) (Figures 1A and 1B). We predicted that if the combination of *RCO* and *KNOX1* expression in leaves represented a preferred developmental path for leaflet formation, then we should repeatedly uncover mutants causing *KNOX1* expression in leaves from this screen. Alternatively, if there was no developmental bias for leaflet formation, then we would uncover mutations in many different pathways previously shown to influence *A. thaliana* leaf complexity.<sup>7,34</sup> From this screen, only four such recessive enhancers were obtained. Notably, all four were novel loss-of-function alleles of the *KNOX1* repressors *AS1* and *AS2* (Figures 1B and 1C; Table S1). We named these alleles *as1-151*, *as1-155*, *as2-163*, and *as2-12*. These alleles have missense mutations that do not change *AS1/AS2* gene expression (Figure S1F). Rosette leaves of *as1-151;RCOg-V*, *as1-155;RCOg-V*, and *as2-163;RCOg-V* mutants displayed terminal and lateral leaflets with bladeless petiolules and rachises, similar to the dissected leaves in *C. hirsuta* (Figures 1A, 1F, 1I, and S1B–S1D), while *as2-12;RCOg-V* showed a weaker phenotype of short petiolules (Figure S1E). Because of the strong leaflet phenotype, we focused on *as1-151;RCOg-V* and *as2-163;RCOg-V* (*as1/2;RCOg-V* in short). We isolated the corresponding single mutants *as1-151* and *as2-163*. Compared to Col-0 wild type, those two single mutants displayed deep serrations and lobes in the basal blade region, but no leaflets (Figures 1E and 1H). Additionally, we quantified the overall form of protrusions (serrations, lobes, and leaflets) in mature leaves by approximating protrusion shapes using triangles whose vertices coincide with the tip and adjoining sinuses of each protrusion. This analysis indicates that the protrusion shapes in *as1/2;RCOg-V* are similar to *C. hirsuta* (long triangles with a narrow base), whereas those of *as1-151/as2-163* and *RCOg-V* are similar to Col-0 (short triangles with a broad base) (Figure 1J). The leaf phenotypes of the double and single mutants suggest that leaflet formation results from a synergistic effect of *as1/as2* mutations and *RCO* expression in leaves. In addition to the leaflet phenotype, we observed shorter

petioles and proximal rachises in *as1;RCOg-V* compared to *as2;RCOg-V* (Figures 1F, 1I, and S1B–S1D). This observation is consistent with the fact that *as1* mutants are more proximodistally compressed than *as2* mutants and display a strong reduction in petiole length.<sup>27,35</sup>

### The leaflet phenotype of *as1/2;RCOg-V* is *KNOX1* dependent

The *AS1/AS2* complex suppresses *BP*, *KNAT2*, and *KNAT6* expression in leaves.<sup>21,26</sup> To understand the contribution of misexpressed *KNOX1* to leaflet formation in *as1/2;RCOg-V* plants, we tested whether the reduction of corresponding *KNOX1* gene activity could suppress leaflet formation in *as1/2;RCOg-V* backgrounds. To this end, we generated *as1-151;RCOg-V;bp-9;kn2-5;kn6-1* quintuple and *as2-163;RCOg-V;bp-9;kn6-1* quadruple mutants (Figure 2A), where the function of *BP*, *KNAT2*, and *KNAT6* was reduced owing to T-DNA insertions in their corresponding genes.<sup>36</sup> To evaluate the contribution of these *KNOX1* genes to *as1/2;RCOg-V* leaf shape, we conducted a multivariate shape analysis.<sup>37</sup> We found that the enhancement of lobes to leaflets in *as1/2;RCOg-V* was largely *KNOX1* dependent (Figures 2B and 2C). Consistent with these results, knocking down *BP*, *KNAT2*, and *KNAT6* in *as1/2;RCOg-V* mutants by an artificial microRNA (*35S<sub>pro</sub>:Amirkn126*) also transformed leaflets into lobes (Figures S2A–S2C). The lobes in *as1-151;RCOg-V;bp-9;kn2-5;kn6-1*, *as2-163;RCOg-V;bp-9;kn6-1*, and *35S<sub>pro</sub>:Amirkn126;as1/2;RCOg-V* were slightly deeper than in *RCOg-V* plants (Figures 2A–2C, S2A, and S2B). Thus, it is possible that residual *KNOX1* activity in these mutants and/or *KNOX1*-independent effects of *AS1/2*, such as those involving *ARF* gene regulation,<sup>38,39</sup> also contribute to leaflet formation. In addition, consistent with the weaker leaf phenotype of the *as2-12;RCOg-V* strain resulting from our screen (Figure S1E), we detected lower *KNOX1* expression in its leaves compared to *as1-151;RCOg-V*, *as1-155;RCOg-V*, and *as2-163;RCOg-V* (Figure S1G).

The above results demonstrate that *KNOX1* expression in leaves is necessary for leaflet formation in *as1/2;RCOg-V* plants. To test whether *BP* expression in the *AS2* domain is also sufficient to generate leaflets together with *RCO*, independently of *as2* mutant alleles, we transformed *RCOg-V* plants with *AtAS2<sub>pro</sub>:AtBP-mCherry*, where *BP-mCherry* was expressed under the *AS2* promoter (Figure S2I). We observed a lobe-to-leaflet transformation in these transgenic plants (Figures S2G and S2H). Nonetheless, *AtAS2<sub>pro</sub>:AtBP-mCherry* plants in wild-type background showed deep serrations/lobes in the basal leaf region, but no leaflets (Figures S2E and S2F), indicating that leaflet formation in transgenic plants requires the combination of *KNOX1* and *RCO* in leaves. Together, these results demonstrate that *KNOX1* expression in leaves is instrumental for generating the leaflet phenotype in *as1/2;RCOg-V*.

### *BP* is misexpressed in the basal midrib/petiole region in *as1/2;RCOg-V*

To investigate the specific pattern of *KNOX1* expression that is associated with leaflet formation in *as1/2;RCOg-V*, we used an *AtBP<sub>pro</sub>:GUS* reporter gene<sup>27</sup> to compare the *BP* transcription pattern in leaf primordia of different lengths (~1,000 μm and ~3,000–5,000 μm) and expanding leaves (~1.5 cm) in Col-0, *as1-151*, *as2-163*, *RCOg-V*, and *as1/2;RCOg-V* mutants

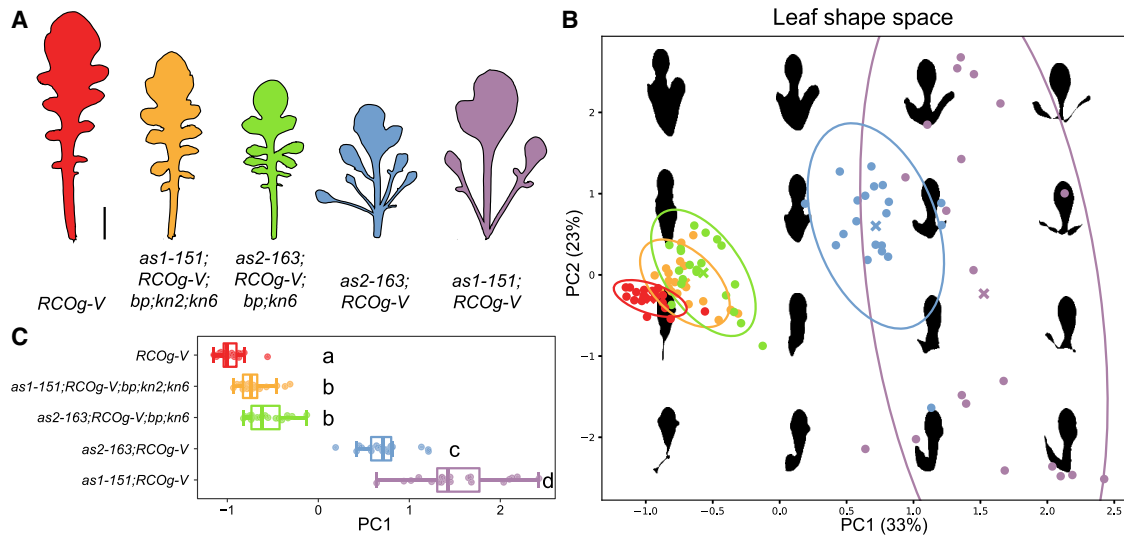


**Figure 2. The leaflet phenotype of *as1/2;RCOg-V* is *KNOX1*-dependent**

(A) Silhouettes of the 11<sup>th</sup> rosette leaves from *RCOg-V*, *as1-151;RCOg-V*, *as1-151;RCOg-V;bp-9;kn2-5;kn6-1*, *as2-163;RCOg-V*, and *as2-163;RCOg-V;bp-9;kn6-1* plants.

(B) Leaf shape space analysis for the genotypes in (A) in Leaf Interrogator<sup>37</sup> of the first two principal components, accounting for 56% of the observed variance. Genotypes are colored as in (A) ( $n = 20$  per genotype). The crosses and eclipses indicate the mean value and standard deviation of each genotype, respectively. The value of principal component 1 (PC1, 33% of the total variance) captures the presence versus absence of leaflets, whereas the value of PC2 (23% of the total variance) captures the degree of bilateral leaf symmetry. The black silhouettes are reconstructed from the principal components to visualize the variation captured by the shape space.

(C) Boxplots to compare the PC1 values of corresponding genotypes in the leaf shape space of (B). Compact letters indicate significant differences (ANOVA combined with Tukey HSD tests,  $p < 0.05$ ).

Scale bars, 1 cm (A). See also Figure S2.

(Figures S3A–S3F and S3). Because *BP*, *KNAT2*, and *KNAT6* were reported to show similar misexpression patterns in *as1* and *as2* mutants,<sup>27,36</sup> we considered *BP* expression in these genotypes as a reasonable proxy for expression of the three genes. We observed no GUS signal in Col-0 and *RCOg-V* rosette leaves (Figures S3A, S3B, S3A, and S3B). Conversely, *AtBP<sub>pro</sub>:GUS* was expressed in the basal midrib/petiole region of *as1-151*, *as2-163*, and *as1/2;RCOg-V* leaf primordia (Figures S3C–S3F) and restricted to the base of petioles in the older leaf primordia (3,000–5,000  $\mu\text{m}$ ) (Figures S3C–S3F). We observed additional foci of *AtBP<sub>pro</sub>:GUS* in the leaflet base of *as1/2;RCOg-V* older leaf primordia (Figures S3D and S3F) and expanding leaves (Figures S3G and S3H). However, these foci are unlikely to be necessary for leaflet formation because we also observed *as2-163;RCOg-V* leaflets without GUS signal foci in all samples (Figure S3I).

These observations of *AtBP<sub>pro</sub>:GUS*, together with the genetic interactions discussed above, indicate that *KNOX1* misexpression at the basal midrib/petiole region of *as1/2;RCOg-V* leaves contributes to leaflet formation. The discrete foci of *AtBP<sub>pro</sub>:GUS* at the *as1/2;RCOg-V* leaflet base were not observed in *as1-151* or *as2-163* leaves (Figures S3C and S3E), suggesting possible crosstalk between *RCO* and *KNOX1* pathways that elevates *KNOX1* expression in *as1/as2* leaves.

#### Expanded *RCO* expression during leaflet patterning in *as1/2;RCOg-V*

To investigate *RCO* expression during leaflet formation in *as1/2;RCOg-V*, we used confocal microscopy to compare the *RCOg-V* fluorescent signal between *as1/2;RCOg-V* and

*RCOg-V* leaf primordia ( $\sim 1,300 \mu\text{m}$  length). We observed that *RCO* expression was limited to the proximal side of the base of developing lobes in *RCOg-V* but expanded into both the proximal and distal sides of the base of developing leaflets in *as1/2;RCOg-V* (Figures S3G–S3I). This bilateral pattern of *RCO* expression in response to ectopic *KNOX1* expression correlated with a narrowing of the leaflet base in *as1/2;RCOg-V* leaves (Figures S3H and S3I), indicating enhanced growth repression by *RCO* in this domain. Leaflet primordia in *AtAS2<sub>pro</sub>:AtBP-mCherry;RCOg-V* showed similar expanded *RCO* expression (Figure S2J). This expanded *RCO* expression domain in the leaflet base resembles that in wild-type *C. hirsuta* leaves,<sup>28</sup> suggesting a common molecular pattern in leaflet development between *A. thaliana as1/2;RCOg-V* mutants and *C. hirsuta*.

#### *KNOX1* confers prolonged growth in the *as2-163* and *as2-163;RCOg-V* leaf basal region

To understand the cell-level basis for leaflet formation in *as1/2;RCOg-V* leaves, we performed live-imaging experiments in developing leaves of Col-0, *as2-163*, *RCOg-V*, and *as2-163;RCOg-V* using confocal microscopy (Figures 4 and 5). We selected *as2-163;RCOg-V* for this live-imaging analysis because its leaf shape is reminiscent of wild-type *C. hirsuta*, in that it does not have the short petioles and proximal rachises observed in *as1-151;RCOg-V* and the reported *C. hirsuta as1* mutant<sup>12</sup> leaves (Figures 1F, 1I, S1B, and S1C). We tracked leaf primordia from 4 to 8 days after initiation (DAI), during which *as2-163;RCOg-V* leaflets grew from initiation to a well-defined morphology with a narrowed base (Figures 4A, 4B, 5A, and 5B; Video S1). Previous

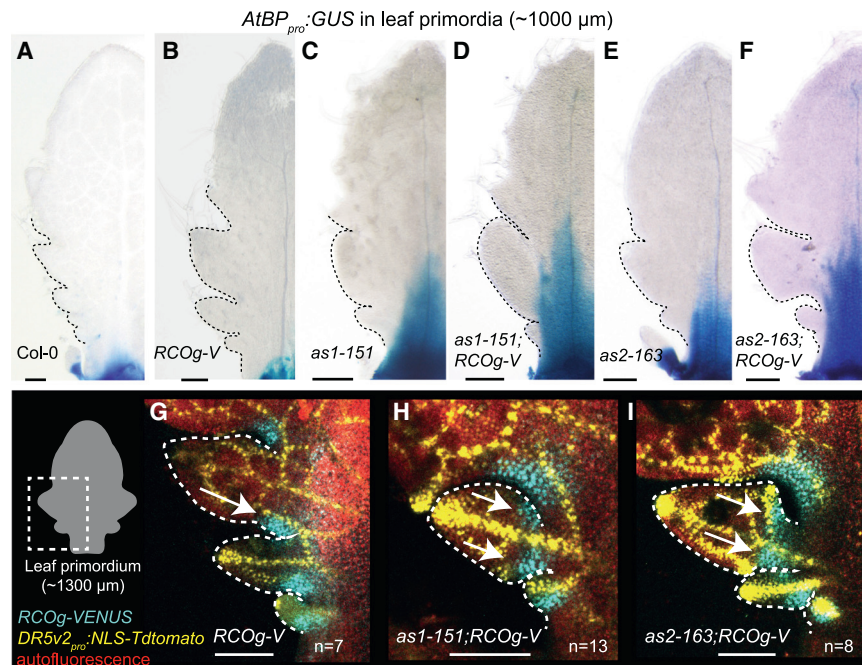


**Figure 3. In *as1/2;RCOg-V*, *BP* is misexpressed in the basal midrib/petiole region and *RCO* expression is expanded in the leaflet base**

(A–F) *AtBP<sub>pro</sub>::GUS* signal in the 10<sup>th</sup> rosette leaf primordia (~1,000 μm length) from 2-week-old Col-0 (A), *RCOg-V* (B), *as1-151* (C), *as1-151;RCOg-V* (D), *as2-163* (E), and *as2-163;RCOg-V* (F) plants (n > 10 per genotype). Protrusion shapes are highlighted with dashed lines.

(G–I) *RCOg-V* expression in the basal region of the 9<sup>th</sup> ± 1 rosette leaf primordia (~1,300 μm length) from 2-week-old *RCOg-V* (G), *as1-151;RCOg-V* (H), and *as2-163;RCOg-V* (I) plants. *RCOg-VENUS* signal (cyan), *DR5v2<sub>pro</sub>::NLS-Tdtomato* signal (yellow), and chlorophyll autofluorescence (red) are presented. *DR5v2* signal marks the tip and veins of protrusions. Dashed lines highlight the protrusion shapes. Arrows indicate the *RCO* expression region in protrusion bases.

Scale bars, 100 μm. See also Figure S3.

results indicated that *KNOX1* expression in leaves prolongs protrusion growth and leads to increased leaf complexity.<sup>16</sup> Thus, we quantified cell growth parameters of area extension (relative growth of cell area) and cell proliferation in corresponding genotypes. Based on the misexpression of *BP* in the basal midrib/petiole region of *as2-163* leaf primordia (Figure 3E), we focused our growth analysis on the basal 25% of cells in each leaf and analyzed the midrib and blade regions separately (Figure 4C). Additionally, we used the cyclin reporter *CYCB1;2<sub>pro</sub>::CYCB1;2-GUS*<sup>40</sup> to monitor patterns of cell proliferation in leaves after the time-lapse window (Figures 4E–4H and S4D–S4G).

While *as2-163* and Col-0 had a broadly similar distribution of cell growth parameters (Figures 4A and 4B), we observed significantly higher area extension in *as2-163* basal midrib cells (after 6 DAI) and increased proliferation in *as2-163* basal midrib/blade cells (6–7 DAI) compared to Col-0 (Figure 4D). Furthermore, we observed a prolonged *CYCB1;2<sub>pro</sub>::CYCB1;2-GUS* signal in basal protrusions of *as2-163* compared to Col-0, after the time-lapse window (~4 mm leaf primordia) (Figures 4F and 4H). Together, these results indicate that growth and proliferation are prolonged in the basal region of *as2-163* leaves, which is consistent with the observed higher outgrowth rate of *as2-163* basal protrusions during the time-lapse window, as well as later leaf development (Figures S4A–S4C). We also observed prolonged cell proliferation in *as2-163;RCOg-V* basal leaf regions compared to *RCOg-V*, as indicated by the *CYCB1;2<sub>pro</sub>::CYCB1;2-GUS* signal at the base of leaflets (Figures S4D–S4G). Overall, these results indicate that *KNOX1*-dependent prolonged cell proliferation contributes to the development of a complex marginal shape in *as2-163* and leaflets in *as2-163;RCOg-V*.

### Elevated anisotropic growth contributes to leaflet formation in *as2-163;RCOg-V*

Rachises and petiolules are major distinguishing shape elements of dissected and simple leaves. To understand the cell growth

properties underpinning the formation of these linear elements in *as2-163;RCOg-V*, we first identified the cell populations giving rise to them, using a reverse cell fate mapping analysis on our time-lapse data. We traced the progeny cells in rachises and petiolules (8 DAI) back to the original cells in young leaf primordia (6 DAI) and found that these two structures originated from cells located at the sinus between protrusions and the protrusion basal region, respectively (Figures 5A and 5C). These specific cell populations grew with higher anisotropy (ratio of the maximal and minimal principal growth directions) compared to *RCOg-V* in the time-lapse window (Figures 5B, 5D, and 5H), with their maximal growth directions unified toward leaf tips (sinus cells) or leaflet tips (protrusion-base cells) (Figure 5B). Quantification of cell growth along the proximal-distal (PD) and medial-lateral (ML) axes of the leaf showed a reduced ML growth rate in sinus cells of *as2-163;RCOg-V* compared to *RCOg-V* (Figures 5E and 5F). Similarly, the protrusion-base cells in *as2-163;RCOg-V* showed reduced growth along the lateral direction relative to the protrusion tip-base PD axis (Figures 5I and 5J). Thus, highly anisotropic cell growth along the PD axis underlies the formation of rachises and petiolules in *as2-163;RCOg-V*. Conversely, *RCOg-V* sinus and protrusion-base cells showed more isotropic growth and contributed to forming leaf blade tissue (Figures 5B–5J and S5C). Consistent with these cell-level observations, quantification of leaflet and lobe shape development using the triangle approximation method presented in Figure 1J confirmed the relative narrowing of the base of leaflets compared to lobes in the time-lapse window (Figure 5K). After the time-lapse window, the anisotropic growth in *as2-163;RCOg-V* petiolules likely persists, as the epidermal cells formed files and elongated toward the tip (Figures S5D and S5E). In short, these observations indicate that a localized wave of anisotropic growth shapes the rachises and petiolules, contributing to leaflet formation in *as2-163;RCOg-V*. These observations are likely relevant to wild-type *C. hirsuta* leaves, because in that genotype, cell growth in rachises was also highly anisotropic (Figures 5L and 5M), as were cell shapes in rachises

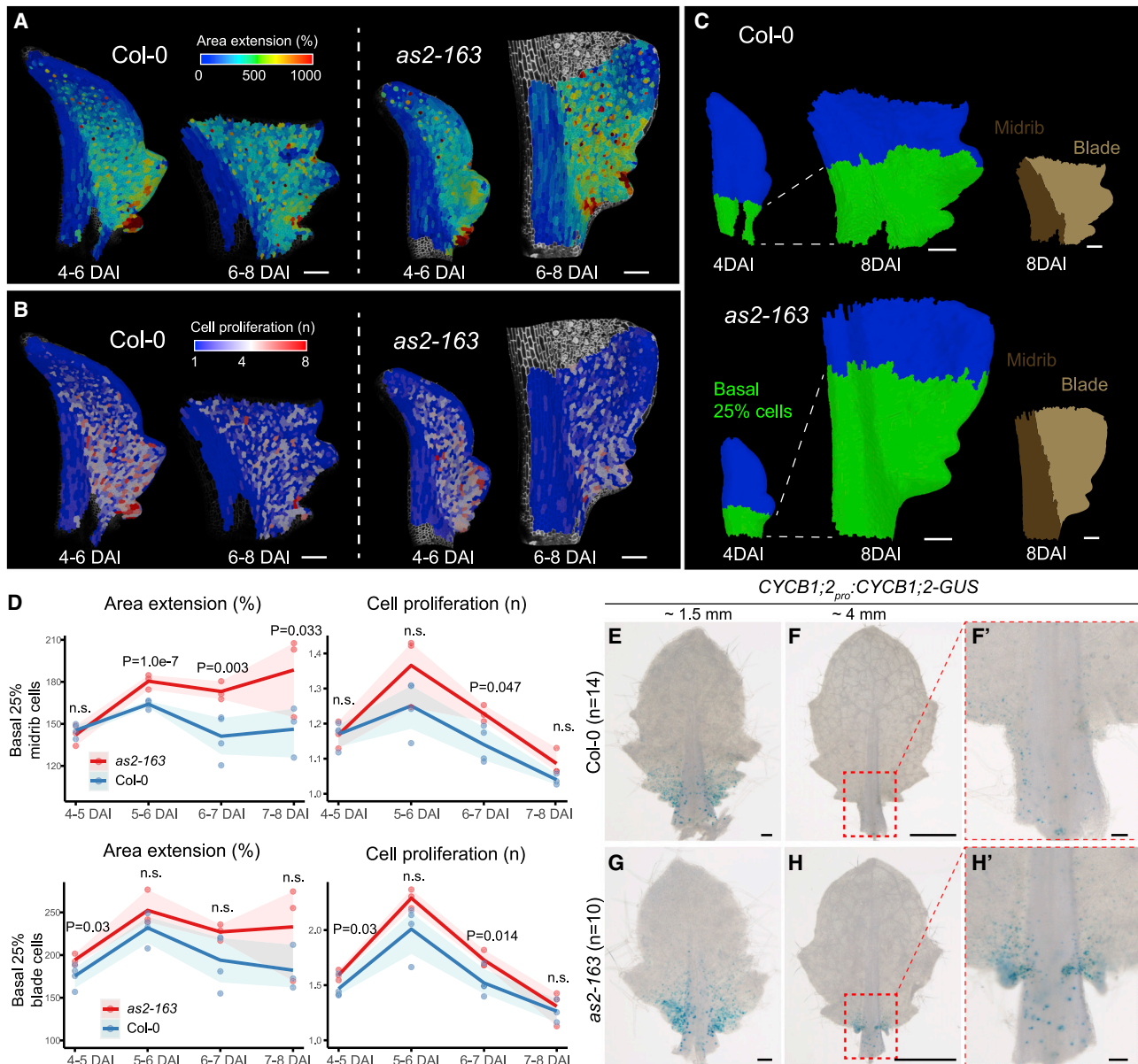


**Figure 4. *KNOX1* confers prolonged growth in the *as2-163* leaf basal region**

(A and B) Heatmaps to show cell area extension (A) and cell proliferation (B) of Col-0 and *as2-163* leaf primordia (leaf node 8<sup>th</sup> ± 1), during 4–6 and 6–8 days after initiation (DAI), visualized on 6 DAI and 8 DAI leaf primordia. The heatmaps for 6–8 DAI only contain the basal parts of leaves.

(C) Left: lineage tracing of basal 25% cells in Col-0 and *as2-163* in 4–8 DAI. Right: midrib and blade regions in leaf primordia.

(D) Comparison of area extension and cell proliferation of basal 25% midrib/blade cells in each time interval between *as2-163* and Col-0. Points indicate the mean values of each sample. Lines and ribbons indicate the mean values and 95% confidence intervals of each genotype. Four samples were analyzed for Col-0 and 3 for *as2-163*, with  $n = 994\text{--}2,300$  cells per sample. Differences in each time interval were tested for significance by nested ANOVA and post hoc comparison. n.s., not significant.

(E–H) *CYCB1;2<sub>pro</sub>::CYCB1;2-GUS* signal in leaf primordia (8<sup>th</sup> and 6<sup>th</sup> leaves, ~1.5 and 4 mm length) from 18-day-old wild-type (E–F) and *as2-163* (G–H) plants. (F') and (H') are magnified images from (F) and (H) to show details at the leaf base.

Scale bars, 100  $\mu\text{m}$  (A–C, E, F', G, and H'); 1 mm (F and H). See also Figures S4 and S6 and Video S1.

and petioles (Figure S5B). Conversely, *C. hirsuta stm-1* mutants, which have reduced *KNOX1* activity and a simplified leaf phenotype (Figure S5A),<sup>14</sup> displayed a more isotropic cell shape in sinuses and lobe bases, similar to those of the lobed leaves in *A. thaliana RCOg-V* plants (Figure S5C). Overall, these results

indicate that *KNOX1* genes exert their effects on dissected leaf shape in part by modulating cell growth anisotropy.

To understand whether the anisotropic growth in *as2-163;RCOg-V* results from *KNOX1* alone or synergy of *KNOX1* and *RCO*, we compared cell growth anisotropy of

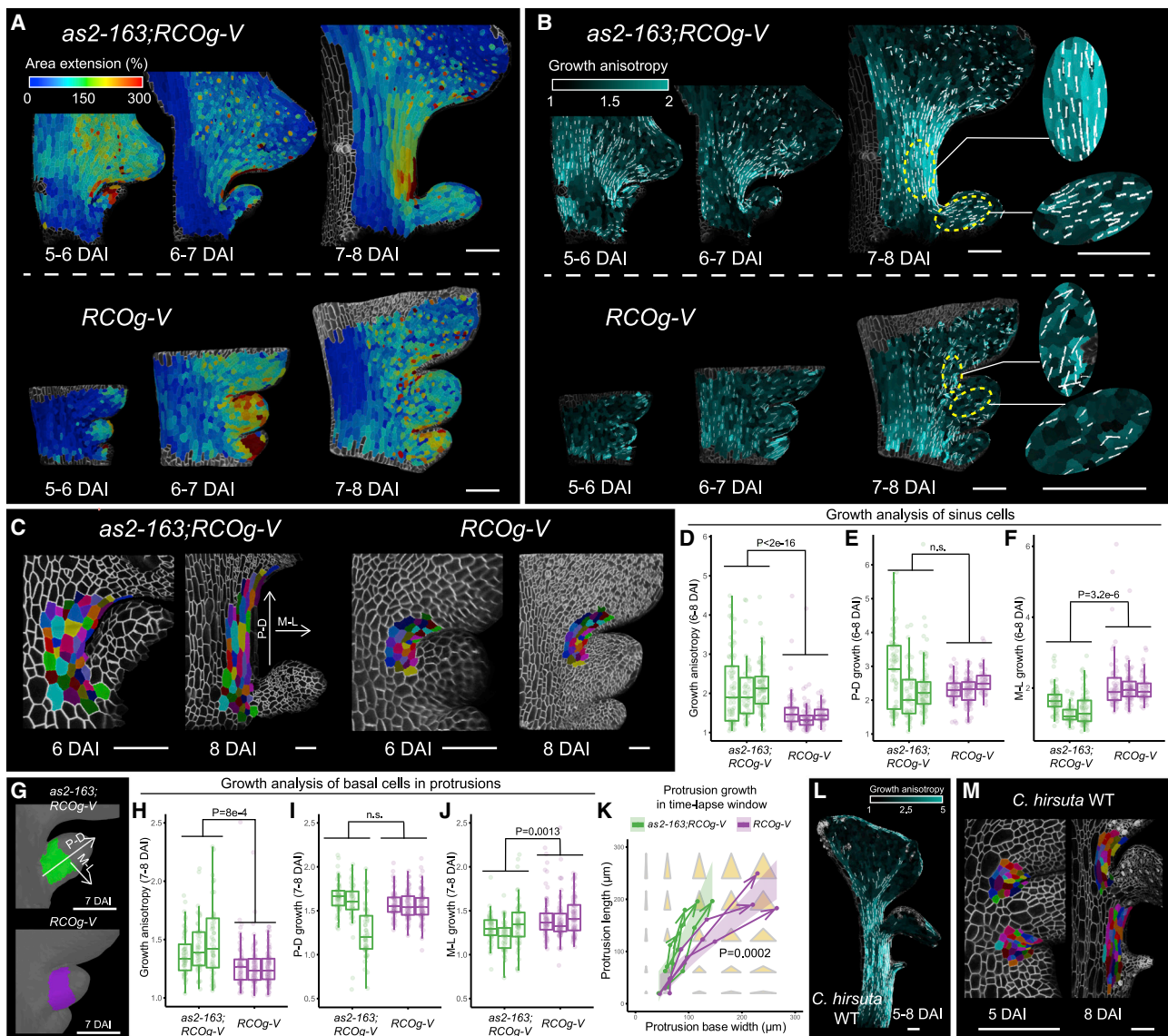


**Figure 5. Elevated anisotropic growth contributes to leaflet formation in *as2-163;RCOg-V***

(A and B) Heatmaps to show cell area extension (A) and growth anisotropy (B) of *as2-163;RCOg-V* and *RCOg-V* leaf primordia, during 5–8 DAI, visualized on the later time point. White lines in (B) indicate maximal cell growth directions where growth anisotropy > 1.3. The sinus and protrusion regions are magnified to show the details.

(C) Cell lineage tracing (6–8 DAI) of sinus cells in *as2-163;RCOg-V* and *RCOg-V* leaf primordia. Colors show the correspondence between cells at 6 DAI and their clonal sectors at 8 DAI. The proximal-distal (PD) and medial-lateral (ML) growth directions are indicated.

(D–F) Quantification of growth anisotropy (D), PD growth rates (E), and ML growth rates (F) of sinus cells in (C), between *as2-163;RCOg-V* and *RCOg-V* (6–8 DAI).

(G) Schematics of protrusion-base cells (colored in green or purple) in *as2-163;RCOg-V* and *RCOg-V*. PD growth to protrusion tips and relative ML growth directions are indicated.

(H–J) Quantification of growth anisotropy (H), PD growth rates (I), and ML growth rates (J) of protrusion base cells in (G).

(K) Protrusion geometry (length versus base width) between *as2-163;RCOg-V* and *RCOg-V* in the time-lapse window. Each arrow represents growth of one sample. Transparent ribbons indicate the 95% confidence intervals based on linear models. The background yellow triangles visualize protrusion shapes. *as2-163;RCOg-V* shows reduced growth in protrusion base width ( $p = 0.0002$ , likelihood ratio test).

(L) Heatmaps to show 5–8 DAI growth anisotropy in *C. hirsuta* wild-type leaf primordia.

(M) Cell lineage tracing of the sinus cells in *C. hirsuta* wild-type leaf primordia in 5–8 DAI.

The 8<sup>th</sup> ± 1 rosette leaf primordia were used for time-lapse and cell growth analysis ( $n = 3$  per genotype). For (C)–(J),  $n = 47$ –82 cells were measured per sample. Differences in (D)–(F) and (H)–(J) were tested for significance by nested ANOVA and post hoc comparison. Scale bars, 50  $\mu\text{m}$  (C); 100  $\mu\text{m}$  (the others). See also [Figures S5](#) and [S6](#) and [Video S1](#).

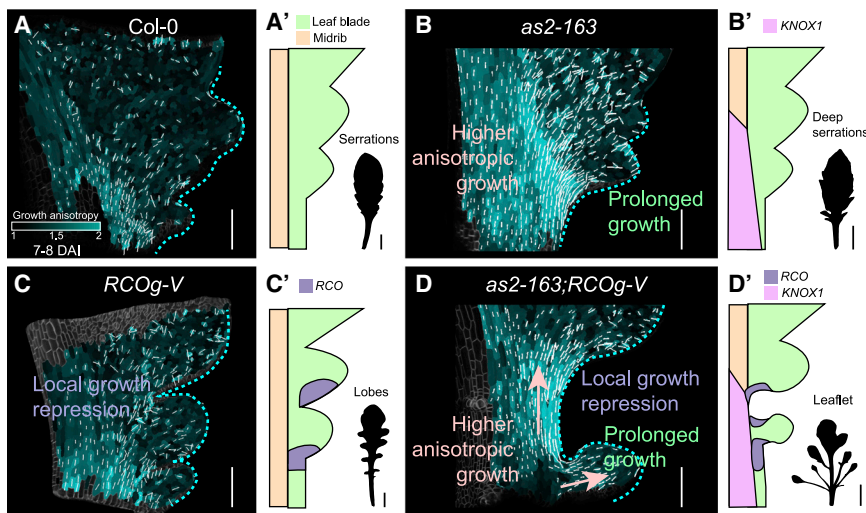


**Figure 6. The synergy between *RCO* and *KNOX1* on cellular growth contributes to leaflet formation in *as2-163;RCOg-V***

(A–D) Heatmaps to show growth anisotropy at the base of leaf primordia of Col-0, *as2-163*, *RCOg-V*, and *as2-163;RCOg-V* (7–8 DAI) plants. White lines indicate maximal cell growth directions where growth anisotropy > 1.3. The cyan dashed lines highlight the leaf marginal shapes.

(A'–D') Schematic diagrams to show the expression pattern of *KNOX1* and *RCO* at the base of leaf primordia and silhouettes of mature leaves from corresponding genotypes.

(A) Col-0 leaves.

(B) *as2-163* leaves show *KNOX1*-mediated prolonged and anisotropic cell growth in the basal region.

(C) The local growth repression by *RCO* produces deep sinuses.

(D) In *as2-163;RCOg-V*, *RCO* expression is expanded into both the proximal and distal sides

of the base of developing leaflets. The synergy between *RCO* and *KNOX1* action elevates growth anisotropy in sinuses and leaflet basal regions, leading to the formation of rachises and petiolules of leaflets, and dissected leaf shapes.

Scale bars, 100  $\mu$ m (A–D); 1 cm (A'–D').

*as2-163;RCOg-V* and *as2-163* to Col-0 in the time-lapse window (Figures S6A–S6C). Both genotypes showed higher growth anisotropy in the basal blade region when analyzed with pooled growth data from all time intervals (Figure S6B). However, in individual time intervals, we observed that *as2-163;RCOg-V*, but not *as2-163*, displayed higher growth anisotropy than Col-0 in the basal blade/midrib region. (Figure S6C). These results indicate that *KNOX1* is sufficient to elevate growth anisotropy in leaf primordia, and this action is enhanced by *RCO* in *as2-163;RCOg-V*. In summary, these observations indicate that *RCO* and *KNOX1* act synergistically to elevate growth anisotropy, which in the context of growth repression by *RCO* and *KNOX1*-mediated growth prolongation (Figures 4D, S4B, and S4C),<sup>16</sup> sculpts leaflets from the emerging leaf blade.

## DISCUSSION

### *RCO* and *KNOX1* action represents a developmentally privileged avenue for leaflet formation

While many genes have the potential to influence trait development, only a subset of them contributes to trait evolution.<sup>2</sup> Prior work has shown that in the case of leaves, *RCO* and *KNOX1* homeobox genes were repeatedly used during evolution to cause diversification of leaf form.<sup>10,11,28,30,41,42</sup> In this work, we asked whether these genes together represented a preferred developmental path for leaflet emergence and what the cellular basis for such a phenomenon might be. As a starting point, we used an *A. thaliana* strain where *RCO* introduction as a transgene partially reversed the loss of *RCO* that occurred in the evolutionary lineage of *A. thaliana*. We showed that upon mutagenizing this strain, *KNOX1* expression in leaves resulting from loss of *AS1/AS2* function caused leaflet formation. The unbiased nature of this experiment and the recovery of solely multiple independent *as1/as2* alleles that can convert lobes to leaflets suggest that in crucifers, the combination of *RCO* and *KNOX1* action in leaves creates a developmentally favored path for leaflet formation.

Our time-lapse analysis further suggests that this “evolutionarily privileged” position of *RCO* and *KNOX1* in crucifer leaflet formation likely reflects their combined ability to control cell and tissue growth: local growth repression, which deepens the sinus region (*RCO*); a prolonged growth window, which allows increased marginal outgrowth (*KNOX1*); and high growth anisotropy, which characterizes the rachis/petiolute for leaf subdivision (*KNOX1*, enhanced by *RCO*) (Figure 6). In species where *RCO* is absent in the genome, an equivalent action might be performed by its paralogs such as *GhLMI1* in cotton<sup>32,43</sup> or other types of genes with local growth repressive action such as the *AUX-IAA* gene *ENTIRE* in tomato.<sup>44</sup>

It is of note that in our screen we recovered mutations in *KNOX1* repressors rather than mutations in *cis*-regulatory regions that caused *KNOX1* expression in leaves. This result likely reflects the fact that core binding motifs of transcription factors are much shorter than gene coding regions, making it more difficult to recover relevant mutations.<sup>45</sup> Mutagenesis with CRISPR-Cas9 coupled with creating chimeras between *A. thaliana* and *C. hirsuta* *KNOX1* regulatory regions will be a good avenue for identifying specific *cis*-elements responsible for the diversification of *KNOX1* expression between the two species.

### *as1/2* mutants highlight a *KNOX1* expression domain sufficient to cause leaflet formation in the presence of *RCO*

Our work indicates that *KNOX1* confers prolonged cell growth and proliferation in *as2-163* leaf primordia (Figures 4D–4H). This result is consistent with previous work that suggests that *STM* expression under the leaf margin promoter *BLS* (*BLS<sub>pro</sub>:STM*) prolongs growth of protrusions.<sup>16</sup> Furthermore, we demonstrated that *KNOX1* expression in leaves elevates growth anisotropy in cells at the base of leaf primordia, thus contributing to the formation of rachises and petiolules in the context of *RCO* (Figures 5B–5J and 6D). In contrast, *as2-163* leaves lack the deep sinus to separate protrusions in the early patterning stage (Figure 6B), while *RCOg-V* leaves lack the

anisotropic growth in the sinus and protrusion base (Figure 6C), resulting in blade formation in the sinus region that connects successive protrusions. Previously, an abstract geometric computational model was reported to simulate diverse compound leaf shapes.<sup>5</sup> In that model, two hypothetical growth factors were invoked to explain the development of the linear geometric elements characterizing compound leaves. The first suppressed lateral growth in sinuses, allowing for the emergence of linear rachises, whereas the second suppressed widening of petiolule bases, allowing them to maintain a linear form despite the elongation of the adjoining rachis.<sup>5</sup> Our results are consistent with this model, as RCO can be considered to capture the first factor while KNOX1 (in synergy with RCO) underlies highly anisotropic cell growth in rachises and petiolules, thus capturing the action of the second factor (Figure 6D). Overall, by incorporating KNOX1 action on anisotropy as a key role in generating linear geometric elements (rachises and petiolules), our work bridges theoretical predictions and experimental observations to understand how cell-level growth properties are translated into complex leaf shapes. These ideas are also broadly consistent with the KNOX1-associated tissue cell polarity switch and anisotropic growth in barley *Hooded* mutant flowers,<sup>46</sup> therefore helping unify interpretations of how KNOX1-mediated effects on cell-level growth properties may influence organ form in diverse systems.

Notably, RCO enhances the effect of KNOX1 on growth anisotropy in *as2-163;RCOg-V* leaves compared to *as2-163* (Figure S6). One possible explanation for this enhancement is that RCO and KNOX1 downstream targets synergistically affect cellular components that set cell growth anisotropy: for example, the cytoskeleton and cell wall. Another explanation might be that local growth repression by RCO in the rachis and petiolule cells reduces physical interconnections between cells, thus accentuating KNOX1 effects on anisotropy.

Another advancement of our results over previous work is that, unlike the deeply lobed leaves of *A. thaliana* *BLS<sub>pro</sub>:STM*,<sup>16,19</sup> *as1-151* and *as2-163* show less severe leaf phenotypes (Figures 1E and 1H) but still enhance RCOg to make leaflets. Compared to *BLS<sub>pro</sub>:STM*, which is expressed along the leaf margin, BP is misexpressed more proximally and medially in the early leaf primordia of *as1-151* and *as2-163*. Thus, these *as1/as2* alleles uncover a phenocritical (here we use “phenocritical” to describe the time and domain of gene expression that is important for a particular gene to regulate development) KNOX1 expression domain at the leaf base that supports leaflet production when RCO is expressed in leaves. This pattern of KNOX1 expression in *as1/as2* leaf primordia is similar to the pattern of *ChSTM* expression in the dissected leaves of *C. hirsuta*,<sup>14,47</sup> highlighting the importance of the proximal and medial part (basal midrib/petiole region) of the leaf primordium for dissected leaf development and evolution. Targeted transgenic approaches, including genetic mosaics and single-cell gene expression profiling, will be required to fully understand the effects of KNOX1 transcription factors on cell-level growth and tissue growth patterns in this domain.

One potential consideration of our studies is that in line with other work in the field,<sup>48</sup> we used the term KNOX1 to collectively refer to *STM*, *BP*, *KNAT2*, and *KNAT6* genes. This designation is justified on the basis of sequence similarity<sup>49</sup> and genetic

evidence for redundancy of these genes, particularly *STM* and *BP*, in meristem maintenance<sup>36,50</sup> and dissected leaf formation.<sup>14</sup> It is also justified by the fact that ectopic expression of different KNOX1 genes in *A. thaliana* leaves generates similar lobed leaf phenotypes,<sup>15,16,51,52</sup> and the result that both *BLS<sub>pro</sub>:STM* and *as1/as2* produce leaflets together with RCO. However, it should be borne in mind that paralogue-specific differences exist in the function of these KNOX1 genes,<sup>53</sup> which need further investigation.

### Crosstalk between RCO and KNOX1 genes

Although previous work indicated that RCO activity does not grossly influence KNOX1 expression (Figures 3B),<sup>28</sup> our genetic results provide evidence for more subtle crosstalk between those genes. First, additional foci of BP expression were observed at the leaflet base in *as1/2;RCOg-V* leaves (Figures S3D and S3F), compared to *as1-151* and *as2-163* (Figures S3C and S3E). Second, RCOg-V expression was expanded to a bilateral pattern in *as1/as2* mutants and the transgenic lines expressing BP under the AS2 promoter (Figures 3G–3I and S2J). Given that KNOX1 and RCO transcription factors both promote cytokinin activity,<sup>29,54,55</sup> and that cytokinin activity may feed back to promote KNOX1 expression,<sup>56,57</sup> it is conceivable that this hormone mediates the KNOX1/RCO crosstalk that we found here. In this context, it will also be interesting to explore whether such crosstalk also promotes STM expression in leaves. Further work in both *A. thaliana* and the endogenous context of *C. hirsuta* will be required to fully investigate the causes and consequences of this crosstalk for leaf morphology, including the precise contribution of the bilateral expression of RCO to leaflet development.

### STAR★METHODS

Detailed methods are provided in the online version of this paper and include the following:

- KEY RESOURCES TABLE
- RESOURCE AVAILABILITY
  - Lead contact
  - Materials availability
  - Data and code availability
- EXPERIMENTAL MODEL AND SUBJECT DETAILS
  - Plant materials and growth conditions
- METHOD DETAILS
  - EMS mutagenesis screen
  - Crossing and genotyping
  - Quantitative PCR
  - β-Glucuronidase (GUS) staining
  - Confocal microscopy
  - Time-lapse experiments and growth analysis
  - Leaf shape and protrusion morphospace analysis
  - Leaf epidermal impressions
  - Plasmid construction and plant transformation
- QUANTIFICATION AND STATISTICAL ANALYSIS

### SUPPLEMENTAL INFORMATION

Supplemental information can be found online at <https://doi.org/10.1016/j.cub.2022.08.020>.

## ACKNOWLEDGMENTS

We thank Angela Hay for helpful discussions and comments on the manuscript, Ismene Karakasilioti for comments on the manuscript, Mohsen Hajheidari for help with the EMS mutagenesis screen, Neha Bhatia and Peter Huijser for help with confocal microscopy, and Esraa Gabal and Ling Dong for technical assistance. This work was supported by a Max Planck Society core grant to M.T.

## AUTHOR CONTRIBUTIONS

Y.W. and M.T. designed experiments. Y.W., S.L., and R.L. performed experiments. S.S. analyzed time-lapse data. B.P. contributed to statistical analysis. A.R. contributed to the leaf shape space analysis. Y.W., S.S., and M.T. wrote the paper with input from the other authors. M.T. designed and directed the study.

## DECLARATION OF INTERESTS

The authors declare no competing interests.

Received: May 27, 2022

Revised: July 28, 2022

Accepted: August 10, 2022

Published: August 26, 2022

## REFERENCES

- Wallace, A. (2004). *Biased Embryos and Evolution* (Cambridge University Press).
- Martin, A., and Orgogozo, V. (2013). The loci of repeated evolution: a catalog of genetic hotspots of phenotypic variation. *Evolution* 67, 1235–1250. <https://doi.org/10.1111/evo.12081>.
- Stern, D.L., and Orgogozo, V. (2009). Is genetic evolution predictable? *Science* 323, 746–751.
- Uller, T., Moczek, A.P., Watson, R.A., Brakefield, P.M., and Laland, K.N. (2018). Developmental bias and evolution: a regulatory network perspective. *Genetics* 209, 949–966. <https://doi.org/10.1534/genetics.118.300995>.
- Runions, A., Tsiantis, M., and Prusinkiewicz, P. (2017). A common developmental program can produce diverse leaf shapes. *New Phytol.* 216, 401–418. <https://doi.org/10.1111/nph.14449>.
- Canales, C., Barkoulas, M., Galinha, C., and Tsiantis, M. (2010). Weeds of change: *Cardamine hirsuta* as a new model system for studying dissected leaf development. *J. Plant Res.* 123, 25–33. <https://doi.org/10.1007/s10265-009-0263-3>.
- Bhatia, N., Runions, A., and Tsiantis, M. (2021). Leaf shape diversity: from genetic modules to computational models. *Annu. Rev. Plant Biol.* 72, 325–356. <https://doi.org/10.1146/annurev-arplant-080720-101613>.
- Long, J.A., Moan, E.I., Medford, J.I., and Barton, M.K. (1996). A member of the KNOTTED class of homeodomain proteins encoded by the *STM* gene of *Arabidopsis*. *Nature* 379, 66–69.
- Vollbrecht, E., Reiser, L., and Hake, S. (2000). Shoot meristem size is dependent on inbred background and presence of the maize homeobox gene. *Development* 127, 3161–3172.
- Bharathan, G., Goliber, T.E., Moore, C., Kessler, S., Pham, T., and Sinha, N.R. (2002). Homologies in leaf form inferred from *KNOX1* gene expression during development. *Science* 296, 1858–1860.
- Hareven, D., Gutfinger, T., Parnis, A., Eshed, Y., and Lifschitz, E. (1996). The making of a compound leaf: genetic manipulation of leaf architecture in tomato. *Cell* 84, 735–744.
- Hay, A., and Tsiantis, M. (2006). The genetic basis for differences in leaf form between *Arabidopsis thaliana* and its wild relative *Cardamine hirsuta*. *Nat. Genet.* 38, 942–947. <https://doi.org/10.1038/ng1835>.
- Piazza, P., Bailey, C.D., Cartolano, M., Krieger, J., Cao, J., Ossowski, S., Schneeberger, K., He, F., de Meaux, J., Hall, N., et al. (2010). *Arabidopsis thaliana* leaf form evolved via loss of *KNOX* expression in leaves in association with a selective sweep. *Curr. Biol.* 20, 2223–2228. <https://doi.org/10.1016/j.cub.2010.11.037>.
- Rast-Somssich, M.I., Broholm, S., Jenkins, H., Canales, C., Vlad, D., Kwantes, M., Bilsborough, G., Ioio, R.D., Ewing, R.M., Laufs, P., et al. (2015). Alternate wiring of a *KNOX1* genetic network underlies differences in leaf development of *A. thaliana* and *C. hirsuta*. *Genes Dev* 29, 2391–2404. <https://doi.org/10.1101/gad.269050>.
- Lincoln, C., Long, J., Yamaguchi, J., Serikawa, K., and Hake, S. (1994). A *knotted1*-like homeobox gene in *Arabidopsis* is expressed in the vegetative meristem and dramatically alters leaf morphology when overexpressed in transgenic plants. *Plant Cell* 6, 1859–1876.
- Kierzkowski, D., Runions, A., Vuolo, F., Strauss, S., Lymbouridou, R., Routier-Kierzkowska, A.L., Wilson-Sánchez, D., Jenke, H., Galinha, C., Mosca, G., et al. (2019). A growth-based framework for leaf shape development and diversity. *Cell* 177, 1405–1418.e17. <https://doi.org/10.1016/j.cell.2019.05.011>.
- Hay, A., Kaur, H., Phillips, A., Hedden, P., Hake, S., and Tsiantis, M. (2002). The gibberellin pathway mediates *KNOTTED1*-Type homeobox function in plants with different body plans. *Curr. Biol.* 12, 1557–1565.
- Chuck, G., Lincoln, C., and Hake, S. (1996). *KNAT1* induces lobed leaves with ectopic meristems when overexpressed in *Arabidopsis*. *Plant Cell* 8, 1277–1289.
- Shani, E., Burko, Y., Ben-Yaakov, L., Berger, Y., Amsellem, Z., Goldshmidt, A., Sharon, E., and Ori, N. (2009). Stage-specific regulation of *Solanum lycopersicum* leaf maturation by class 1 *KNOTTED1*-LIKE *HOMEOBOX* proteins. *Plant Cell* 21, 3078–3092. <https://doi.org/10.1105/tpc.109.068148>.
- Hay, A., Jackson, D., Ori, N., and Hake, S. (2003). Analysis of the competence to respond to *KNOTTED1* activity in *Arabidopsis* leaves using a steroid induction system. *Plant Physiol.* 131, 1671–1680. <https://doi.org/10.1104/pp.102.017434>.
- Byrne, M.E., Barley, R., Curtis, M., Arroyo, J.M., Dunham, M., Hudson, A., and Martienssen, R.A. (2000). *Asymmetric leaves1* mediates leaf patterning and stem cell function in *Arabidopsis*. *Nature* 408, 967–971.
- Schneeberger, R., Tsiantis, M., Freeling, M., and Langdale, J.A. (1998). The *rough sheath2* gene negatively regulates homeobox gene expression. *Development* 125, 2857–2865.
- Waites, R., Selvadurai, H.R., Oliver, I.R., and Hudson, A. (1998). The *PHANTASTICA* gene encodes a MYB transcription factor involved in growth and dorsoventrality of lateral organs in *Antirrhinum*. *Cell* 93, 779–789.
- Tsiantis, M., Schneeberger, R., Golz, J.F., Freeling, M., and Langdale, J.A. (1999). The maize *rough sheath2* gene and leaf development programs in monocot and dicot plants. *Science* 284, 154–156.
- Semiarti, E., Ueno, Y., Tsukaya, H., Iwakawa, H., Machida, C., and Machida, Y. (2001). The *ASYMMETRIC LEAVES2* gene of *Arabidopsis thaliana* regulates formation of a symmetric lamina, establishment of venation and repression of meristem-related homeobox genes in leaves. *Development* 128, 1771–1783.
- Guo, M., Thomas, J., Collins, G., and Timmermans, M.C.P. (2008). Direct repression of *KNOX* loci by the *ASYMMETRIC LEAVES1* complex of *Arabidopsis*. *Plant Cell* 20, 48–58. <https://doi.org/10.1105/tpc.107.056127>.
- Ori, N., Eshed, Y., Chuck, G., Bowman, J.L., and Hake, S. (2000). Mechanisms that control *knox* gene expression in the *Arabidopsis* shoot. *Development* 127, 5523–5532.
- Vlad, D., Kierzkowski, D., Rast, M.I., Vuolo, F., Dello Ioio, R., Galinha, C., Gan, X., Hajheidari, M., Hay, A., Smith, R.S., et al. (2014). Leaf shape evolution through duplication, regulatory diversification, and loss of a homeobox gene. *Science* 343, 780–783.

29. Hajheidari, M., Wang, Y., Bhatia, N., Vuolo, F., Franco-Zorrilla, J.M., Karady, M., Mentink, R.A., Wu, A., Oluwatobi, B.R., Müller, B., et al. (2019). Autoregulation of *RCO* by low-affinity binding modulates cytokinin action and shapes leaf diversity. *Curr. Biol.* 29, 4183–4192.e6. <https://doi.org/10.1016/j.cub.2019.10.040>.
30. Sicard, A., Thamm, A., Marona, C., Lee, Y.W., Wahl, V., Stinchcombe, J.R., Wright, S.I., Kappel, C., and Lenhard, M. (2014). Repeated evolutionary changes of leaf morphology caused by mutations to a homeobox gene. *Curr. Biol.* 24, 1880–1886. <https://doi.org/10.1016/j.cub.2014.06.061>.
31. Hu, L., Zhang, H., Yang, Q., Meng, Q., Han, S., Nwafor, C.C., Khan, M.H.U., Fan, C., and Zhou, Y. (2018). Promoter variations in a homeobox gene, *BnA10.LMI1*, determine lobed leaves in rapeseed (*Brassica napus* L.). *Theor. Appl. Genet.* 131, 2699–2708. <https://doi.org/10.1007/s00122-018-3184-5>.
32. Andres, R.J., Coneva, V., Frank, M.H., Tuttle, J.R., Samayoa, L.F., Han, S.W., Kaur, B., Zhu, L., Fang, H., Bowman, D.T., et al. (2017). Modifications to a *LATE MERISTEM IDENTITY1* gene are responsible for the major leaf shapes of Upland cotton (*Gossypium hirsutum* L.). *Proc. Natl. Acad. Sci. USA* 114, E57–E66. <https://doi.org/10.1073/pnas.1613593114>.
33. Vuolo, F., Mentink, R.A., Hajheidari, M., Bailey, C.D., Filatov, D.A., and Tsiantis, M. (2016). Coupled enhancer and coding sequence evolution of a homeobox gene shaped leaf diversity. *Genes Dev.* 30, 2370–2375. <https://doi.org/10.1101/gad.290684.116>.
34. Blein, T., Pautot, V., and Laufs, P. (2013). Combinations of mutations sufficient to alter *Arabidopsis* leaf dissection. *Plants* 2, 230–247. <https://doi.org/10.3390/plants2020230>.
35. Ikezaki, M., Kojima, M., Sakakibara, H., Kojima, S., Ueno, Y., Machida, C., and Machida, Y. (2010). Genetic networks regulated by *ASYMMETRIC LEAVES1* (*AS1*) and *AS2* in leaf development in *Arabidopsis thaliana*: *KNOX* genes control five morphological events. *Plant J.* 61, 70–82. <https://doi.org/10.1111/j.1365-313X.2009.04033.x>.
36. Belles-Boix, E., Hamant, O., Witiak, S.M., Morin, H., Traas, J., and Pautot, V. (2006). *KNAT6*: an *Arabidopsis* homeobox gene involved in meristem activity and organ separation. *Plant Cell* 18, 1900–1907. <https://doi.org/10.1105/tpc.106.041988>.
37. Zhang, Z., Runions, A., Mentink, R.A., Kierzkowski, D., Karady, M., Hashemi, B., Huijser, P., Strauss, S., Gan, X., Ljung, K., and Tsiantis, M. (2020). A *WOX/Auxin* biosynthesis module controls growth to shape leaf form. *Curr. Biol.* 30, 4857–4868.e6. <https://doi.org/10.1016/j.cub.2020.09.037>.
38. Iwasaki, M., Takahashi, H., Iwakawa, H., Nakagawa, A., Ishikawa, T., Tanaka, H., Matsumura, Y., Pekker, I., Eshed, Y., Vial-Pradel, S., et al. (2013). Dual regulation of *ETTIN* (*ARF3*) gene expression by *AS1-AS2*, which maintains the DNA methylation level, is involved in stabilization of leaf adaxial-abaxial partitioning in *Arabidopsis*. *Development* 140, 1958–1969. <https://doi.org/10.1242/dev.085365>.
39. Husbands, A.Y., Benkovics, A.H., Nogueira, F.T.S., Lodha, M., and Timmermans, M.C.P. (2015). The *ASYMMETRIC LEAVES* complex employs multiple modes of regulation to affect adaxial-abaxial patterning and leaf complexity. *Plant Cell* 27, 3321–3335. <https://doi.org/10.1105/tpc.15.00454>.
40. Donnelly, P.M., Bonetta, D., Tsukaya, H., Dengler, R.E., and Dengler, N.G. (1999). Cell cycling and cell enlargement in developing leaves of *Arabidopsis*. *Dev. Biol.* 215, 407–419.
41. Hay, A., and Tsiantis, M. (2010). *KNOX* genes: versatile regulators of plant development and diversity. *Development* 137, 3153–3165. <https://doi.org/10.1242/dev.030049>.
42. Kimura, S., Koenig, D., Kang, J., Yoong, F.Y., and Sinha, N. (2008). Natural variation in leaf morphology results from mutation of a novel *KNOX* gene. *Curr. Biol.* 18, 672–677. <https://doi.org/10.1016/j.cub.2008.04.008>.
43. Chang, L., Mei, G., Hu, Y., Deng, J., and Zhang, T. (2019). *LMI1*-like and *KNOX1* genes coordinately regulate plant leaf development in dicotyledons. *Plant Mol. Biol.* 99, 449–460. <https://doi.org/10.1007/s11103-019-00829-7>.
44. Israeli, A., Capua, Y., Shwartz, I., Tal, L., Meir, Z., Levy, M., Bar, M., Efroni, I., and Ori, N. (2019). Multiple auxin-response regulators enable stability and variability in leaf development. *Curr. Biol.* 29, 1746–1759.e5. <https://doi.org/10.1016/j.cub.2019.04.047>.
45. Jander, G., Baerson, S.R., Hudak, J.A., Gonzalez, K.A., Gruys, K.J., and Last, R.L. (2003). Ethylmethanesulfonate saturation mutagenesis in *Arabidopsis* to determine frequency of herbicide resistance. *Plant Physiol.* 131, 139–146. <https://doi.org/10.1104/pp.102.010397>.
46. Richardson, A., Rebocho, A.B., and Coen, E. (2016). Ectopic *KNOX* expression affects plant development by altering tissue cell polarity and identity. *Plant Cell* 28, 2079–2096. <https://doi.org/10.1105/tpc.16.00284>.
47. Barkoulas, M., Hay, A., Kougioumoutzi, E., and Tsiantis, M. (2008). A developmental framework for dissected leaf formation in the *Arabidopsis* relative *Cardamine hirsuta*. *Nat. Genet.* 40, 1136–1141. <https://doi.org/10.1038/ng.189>.
48. Furumizu, C., Alvarez, J.P., Sakakibara, K., and Bowman, J.L. (2015). Antagonistic roles for *KNOX1* and *KNOX2* genes in patterning the land plant body plan following an ancient gene duplication. *PLoS Genet.* 11, e1004980. <https://doi.org/10.1371/journal.pgen.1004980>.
49. Hake, S., Smith, H.M.S., Holtan, H., Magnani, E., Mele, G., and Ramirez, J. (2004). The role of *knox* genes in plant development. *Annu. Rev. Cell Dev. Biol.* 20, 125–151. <https://doi.org/10.1146/annurev.cellbio.20.031803.093824>.
50. Byrne, M.E., Simorowski, J., and Martienssen, R.A. (2002). *ASYMMETRIC LEAVES1* reveals *knox* gene redundancy in *Arabidopsis*. *Development* 129, 1957–1965.
51. Pautot, V., Dockx, J., Hamant, O., Kronenberger, J., Grandjean, O., Jublot, D., and Traas, J. (2001). *KNAT2*: evidence for a link between knotted-like genes and carpel development. *Plant Cell* 13, 1719–1734.
52. Dean, G., Casson, S., and Lindsey, K. (2004). *KNAT6* gene of *Arabidopsis* is expressed in roots and is required for correct lateral root formation. *Plant Mol. Biol.* 54, 71–84.
53. Hay, A., and Tsiantis, M. (2009). A *KNOX* family TALE. *Curr. Opin. Plant Biol.* 12, 593–598. <https://doi.org/10.1016/j.pbi.2009.06.006>.
54. Jasinski, S., Piazza, P., Craft, J., Hay, A., Woolley, L., Rieu, I., Phillips, A., Hedden, P., and Tsiantis, M. (2005). *KNOX* action in *Arabidopsis* is mediated by coordinate regulation of cytokinin and gibberellin activities. *Curr. Biol.* 15, 1560–1565. <https://doi.org/10.1016/j.cub.2005.07.023>.
55. Yanai, O., Shani, E., Dolezal, K., Tarkowski, P., Sablowski, R., Sandberg, G., Samach, A., and Ori, N. (2005). *Arabidopsis* *KNOX1* proteins activate cytokinin biosynthesis. *Curr. Biol.* 15, 1566–1571. <https://doi.org/10.1016/j.cub.2005.07.060>.
56. Rupp, H.-M., Frank, M., Werner, T., Strnad, M., and Schumüller, T. (1999). Increased steady state mRNA levels of the *STM* and *KNAT1* homeobox genes in cytokinin overproducing *Arabidopsis thaliana* indicate a role for cytokinins in the shoot apical meristem. *Plant J.* 18, 557–563.
57. Kurakawa, T., Ueda, N., Maekawa, M., Kobayashi, K., Kojima, M., Nagato, Y., Sakakibara, H., and Kyoizuka, J. (2007). Direct control of shoot meristem activity by a cytokinin-activating enzyme. *Nature* 445, 652–655. <https://doi.org/10.1038/nature05504>.
58. Segonzac, C., Nimchuk, Z.L., Beck, M., Tarr, P.T., Robatzek, S., Meyerowitz, E.M., and Zipfel, C. (2012). The shoot apical meristem regulatory peptide *CLV3* does not activate innate immunity. *Plant Cell* 24, 3186–3192. <https://doi.org/10.1105/tpc.111.091264>.
59. Schindelin, J., Arganda-Carreras, I., Frise, E., Kaynig, V., Longair, M., Pietzsch, T., Preibisch, S., Rueden, C., Saalfeld, S., Schmid, B., et al. (2012). Fiji: an open-source platform for biological-image analysis. *Nat. Methods* 9, 676–682. <https://doi.org/10.1038/nmeth.2019>.
60. Barbier de Reuille, P., Routier-Kierzkowska, A.-L., Kierzkowski, D., Bassel, G.W., Schüpbach, T., Tauriello, G., Bajpai, N., Strauss, S., Weber, A., Kiss, A., et al. (2015). MorphoGraphX: a platform for quantifying morphogenesis in 4D. *eLife* 4, e05864. <https://doi.org/10.7554/eLife.05864>.

61. R Core Team (2021). R: A language and environment for statistical computing (R Foundation for Statistical Computing).
62. Wickham, H. (2016). *ggplot2: Elegant Graphics for Data Analysis* (Springer-Verlag).
63. Strauss, S., Runions, A., Lane, B., Eschweiler, D., Bajpai, N., Trozzi, N., Routier-Kierzkowska, A.-L., Yoshida, S., Rodrigues da Silveira, S., Vijayan, A., et al. (2022). Using positional information to provide context for biological image analysis with MorphoGraphX 2.0. *eLife* *11*, e72601.
64. Strauss, S., Sapala, A., Kierzkowski, D., and Smith, R.S. (2019). Quantifying plant growth and cell proliferation with MorphoGraphX. *Methods Mol. Biol.* *1992*, 269–290. [https://doi.org/10.1007/978-1-4939-9469-4\\_18](https://doi.org/10.1007/978-1-4939-9469-4_18).
65. Clough, S.J., and Bent, A.F. (1998). Floral dip: a simplified method for *Agrobacterium* -mediated transformation of *Arabidopsis thaliana*. *Plant J.* *16*, 735–743. <https://doi.org/10.1046/j.1365-313x.1998.00343.x>.

STAR★METHODS

KEY RESOURCES TABLE

REAGENT or RESOURCE	SOURCE	IDENTIFIER
<b>Chemicals, peptides, and recombinant proteins</b>		
Ethyl methanesulfonate (EMS)	Sigma-Aldrich	Cat#M0880
X-gluc	Roth	Cat#0018
Mango Taq	Bioline	Cat#BIO-21083
Phusion High-Fidelity DNA Polymerase	NEB	Cat#M0530
½ MS Medium including vitamins	Duchefa Biochem	Cat#M0222.0050
Hygromycin	Roth	Cat#CP12.1
Plant Preservative Mixture (PPM)	Plant Cell Technology	250
<b>Critical commercial assays</b>		
RNeasy Plant Mini Kit	QIAGEN	Cat#74904
SuperScript VILO cDNA Synthesis Kit	Invitrogen	Cat#11754050
Power SYBR Green PCR Master Mix	Thermo Fisher Scientific	Cat#4367659
<b>Experimental models: Organisms/strains</b>		
<i>A. thaliana</i> : wild type Col-0	NASC	N60000
<i>A. thaliana</i> : RCO <sub>pro</sub> :RCOg-VENUS (RCOg-V)	Vuolo et al. <sup>33</sup>	N/A
<i>A. thaliana</i> : as1-151;RCOg-V	This study	N/A
<i>A. thaliana</i> : as1-155;RCOg-V	This study	N/A
<i>A. thaliana</i> : as2-163;RCOg-V	This study	N/A
<i>A. thaliana</i> : as2-12;RCOg-V	This study	N/A
<i>A. thaliana</i> : as1-151	This study	N/A
<i>A. thaliana</i> : as2-163	This study	N/A
<i>A. thaliana</i> : as1-1	Semiarti et al. <sup>25</sup>	CS3374
<i>A. thaliana</i> : as2-1	Semiarti et al. <sup>25</sup>	CS3117
<i>A. thaliana</i> : bp-9;kn2-5;kn6-1	Belles-Boix et al. <sup>36</sup>	N/A
<i>A. thaliana</i> : as1-151;RCOg-V;bp-9;kn2-5;kn6-1	This study	N/A
<i>A. thaliana</i> : as2-163;RCOg-V;bp-9;kn6-1	This study	N/A
<i>A. thaliana</i> : as1-151;RCOg-V;35S <sub>pro</sub> :Amirkn126	This study	N/A
<i>A. thaliana</i> : as2-163;RCOg-V;35S <sub>pro</sub> :Amirkn126	This study	N/A
<i>A. thaliana</i> : as1-151;RCOg-V;ev(pML-Hyg)	This study	N/A
<i>A. thaliana</i> : as2-163;RCOg-V;ev(pML-Hyg)	This study	N/A
<i>A. thaliana</i> : AtAS2 <sub>pro</sub> :AtBP-mCherry;RCOg-V	This study	N/A
<i>A. thaliana</i> : AtAS2 <sub>pro</sub> :AtBP-mCherry	This study	N/A
<i>A. thaliana</i> : AtBP <sub>pro</sub> :GUS	Ori et al. <sup>27</sup>	N/A
<i>A. thaliana</i> : as1-151;AtBP <sub>pro</sub> :GUS	This study	N/A
<i>A. thaliana</i> : as2-163;AtBP <sub>pro</sub> :GUS	This study	N/A
<i>A. thaliana</i> : as1-151;RCOg-V;AtBP <sub>pro</sub> :GUS	This study	N/A
<i>A. thaliana</i> : as2-163;RCOg-V;AtBP <sub>pro</sub> :GUS	This study	N/A
<i>A. thaliana</i> : RCOg-V;AtBP <sub>pro</sub> :GUS	This study	N/A
<i>A. thaliana</i> : DR5v2 <sub>pro</sub> :Tdtomato	Zhang et al. <sup>37</sup>	N/A
<i>A. thaliana</i> : RCOg-V;DR5v2 <sub>pro</sub> :Tdtomato	This study	N/A
<i>A. thaliana</i> : as1-151;RCOg-V;DR5v2 <sub>pro</sub> :Tdtomato	This study	N/A
<i>A. thaliana</i> : as2-163;RCOg-V;DR5v2 <sub>pro</sub> :Tdtomato	This study	N/A
<i>A. thaliana</i> : UBQ10 <sub>pro</sub> :PM-Tdtomato	Segonzac et al. <sup>58</sup>	N/A
<i>A. thaliana</i> : as2-163;UBQ10 <sub>pro</sub> :PM-Tdtomato	This study	N/A

(Continued on next page)

**Continued**

REAGENT or RESOURCE	SOURCE	IDENTIFIER
<i>A. thaliana</i> : RCOg-V;UBQ10 <sub>pro</sub> :PM-Tdtomato	This study	N/A
<i>A. thaliana</i> : as2-163;RCOg-V;UBQ10 <sub>pro</sub> :PM-Tdtomato	This study	N/A
<i>A. thaliana</i> : CYCB1;2 <sub>pro</sub> :CYCB1;2-GUS	Donnelly et al. <sup>40</sup>	N/A
<i>A. thaliana</i> : as2-163;CYCB1;2 <sub>pro</sub> :CYCB1;2-GUS	This study	N/A
<i>A. thaliana</i> : RCOg-V;CYCB1;2 <sub>pro</sub> :CYCB1;2-GUS	This study	N/A
<i>A. thaliana</i> : as2-163;RCOg-V;CYCB1;2 <sub>pro</sub> :CYCB1;2-GUS	This study	N/A
<i>C. hirsuta</i> : wild type Oxford	N/A	N/A
<i>C. hirsuta</i> : <i>chstm-1</i>	Rast-Somssich et al. <sup>14</sup>	N/A
<b>Oligonucleotides</b>		
All the oligonucleotides	This study	Table S2
<b>Recombinant DNA</b>		
<i>pML-Hyg-35S<sub>pro</sub>:Amikn126</i>	This study	N/A
<i>pML-Hyg-AtAS2<sub>pro</sub>:AtBP-mCherry</i>	This study	N/A
<b>Software and algorithms</b>		
Leica application suite X	Leica	<a href="https://www.leica-microsystems.com/products/microscope-software/p/leica-las-x-ls/">https://www.leica-microsystems.com/products/microscope-software/p/leica-las-x-ls/</a>
Fiji (ImageJ 1.53q)	Schindelin et al. <sup>59</sup>	<a href="https://fiji.sc/">https://fiji.sc/</a>
MorphoGraphX (MGX) (version 2.0)	Barbier de Reuille et al. <sup>60</sup>	<a href="https://morphographx.org/">https://morphographx.org/</a>
Leaf Interrogator (LeafI)	Zhang et al. <sup>37</sup>	<a href="https://gitlab.mpcdf.mpg.de/g-adamrunions/leafinterrogator_zhang_et_al">https://gitlab.mpcdf.mpg.de/g-adamrunions/leafinterrogator_zhang_et_al</a>
R (version 4.1.1)	R Core Team <sup>61</sup>	<a href="https://www.r-project.org/">https://www.r-project.org/</a>
R package: ggplot2 (version 3.3.5)	Wickham et al. <sup>62</sup>	<a href="https://ggplot2.tidyverse.org/">https://ggplot2.tidyverse.org/</a>
FFmpeg (version 5.0)	FFmpeg	<a href="https://ffmpeg.org/">https://ffmpeg.org/</a>

**RESOURCE AVAILABILITY**

**Lead contact**

Further information and requests for resources and reagents should be directed to and will be fulfilled by the lead contact Milto Tsiantis ([tsiantis@mpipz.mpg.de](mailto:tsiantis@mpipz.mpg.de)).

**Materials availability**

All unique/stable reagents generated in this study are available from the lead contact with a completed Materials Transfer Agreement.

**Data and code availability**

- Microscopy data reported in this paper will be shared by the lead contact upon request.
- This paper does not report original code.
- Any additional information required to reanalyze the data reported in this paper is available from the lead contact upon request.

**EXPERIMENTAL MODEL AND SUBJECT DETAILS**

**Plant materials and growth conditions**

*A. thaliana* and *C. hirsuta* plant materials were listed in [key resources table](#). Soil-grown plants were cultivated in greenhouses under long-day conditions (16-hour light: 8-hour dark, with supplemental lighting when nature light intensity was below 75  $\mu\text{mol m}^{-2} \text{s}^{-1}$ ) at 22°C, except for *chstm-1*<sup>14</sup> which was cultivated in climate chambers (Reftech) under short-day conditions [8-hour light (20°C): 16-hour dark (18°C), light intensity 110  $\mu\text{mol m}^{-2} \text{s}^{-1}$ , humidity 65%] to promote leaf generation (Figure S5). *A. thaliana* seeds were cold-stratified within 1/1000 agar solutions (w/v) at 4°C for two days, then pipetted to wet soil surface to grow. *C. hirsuta* seeds were sowed on wet soil surface, cold-stratified at 4°C for one week, then grown in the greenhouse. For hygromycin-resistance screen, *A. thaliana* seeds were sterilized by 70% ethanol (v/v), sowed on ½ MS plates with 1.5% plant agar (w/v) and 25 mg/L hygromycin (Roth), stratified at 4°C for two days, then grown in climate chambers (Reftech) under long-day conditions [16-hour light (20°C): 8-hour dark (18°C), light intensity 110  $\mu\text{mol m}^{-2} \text{s}^{-1}$ , humidity 65%].

For time-lapse experiments, about 17 day-after-sowing old *A. thaliana* soil-grown plants were used, and their cotyledons/older leaves were removed to expose the 8<sup>th</sup> ± 1 rosette leaves for imaging. The dissected plants were then transferred into Ø60mm Petri

dishes filled with ½ MS Medium including vitamins (Duchefa Biochem), supplemented with 1.5% plant agar (w/v), 1% sucrose (w/v) and 0.1 % Plant Preservative Mixture (Plant Cell Technology, v/v). Between imaging, plants were transferred to growth chambers and cultured *in vitro* under long-day conditions as described above.

## METHOD DETAILS

### EMS mutagenesis screen

EMS mutagenesis was performed in homozygous *RCOg-VENUS* transgenic seeds (*A. thaliana* Col-0 ecotype)<sup>33</sup> by treating the seeds with 100mM EMS (Sigma) for 4 hours (M1 seeds). M1 plants were self-pollinated to generate the M2 seeds. M2 seeds were harvested in pools of five plants. 220 pools (1100 M2 families) and 216 plants per pool were screened and four enhancers were obtained with leaflet phenotypes. *AS1* and *AS2* were considered as candidates because of the phenotypic similarity of those enhancers to a previously reported *C. hirsuta as1* mutant.<sup>12</sup> We performed Sanger sequencing to identify the mutation sites of *as1-151*, *as1-155*, *as2-163* and *as2-12*, and this was followed by allelism tests. *as1-151;RCOg-V* and *as2-163;RCOg-V* were backcrossed to *RCOg-V* twice to remove background mutations. *as1-155;RCOg-V* and *as2-12;RCOg-V* were backcrossed to *RCOg-V* once. For allelism tests, the *as1/as2* mutants obtained from the screen were crossed with *as1-1* (CS3374) and *as2-1* (CS3117).<sup>25</sup>

### Crossing and genotyping

*atbp-9;knat2-5;knat6-1*<sup>36</sup> was crossed to *as1-151;RCOg-V* or *as2-163;RCOg-V* mutants. F1 plants were self-pollinated to generate the F2 populations. F2, F3 and F4 populations were genotyped to obtain *as1-151;RCOg-V;bp-9;kn2-5;kn6-1* quintuple and *as2-163;RCOg-V;bp-9;kn6-1* quadruple mutants. The F4 plants were used for leaf shape analysis. A CAPS marker was designed to genotype *as1-151* (*as1-151\_gt\_F* and *as1-151\_gt\_R*, *XmaI* to cut the wild-type PCR product), and a dCAPS marker was used to genotype *as2-163* (*as2-163\_gt\_F* and *as2-163\_gt\_R*, *PstI* to cut the wild-type PCR product). For *bp-9*, *BP-14* and *new\_BP-3* were used to amplify the wild-type band (2kbp), while *BP-14* and *dSpm1* for the mutant band (1.5kbp). For *knat2-5*, *knat2-5\_LP* and *knat2-5\_RP* were used to amplify the wild-type band (1.5kbp), while *knat2-5\_RP* and *JMLB1* for the mutant band (1kbp). For *knat6-1*, *knat6-1\_LP* and *knat6-1\_RP* were used to amplify the wild-type band (1.5kbp), while *knat6-1\_RP* and *JMLB1* for the mutant band (1kbp). All PCRs were performed using Mango Taq polymerase (Bioline) except for the *bp-9* wild-type band where we used Phusion polymerase (NEB). The primers used for genotyping are listed in Table S2.

*AtBP<sub>pro</sub>:GUS* homozygous plants<sup>27</sup> were crossed to *as1-151;RCOg-V* or *as2-163;RCOg-V* mutants. Homozygous *as1-151;AtBP<sub>pro</sub>:GUS*, *as2-163;AtBP<sub>pro</sub>:GUS*, *as1-151;RCOg-V;AtBP<sub>pro</sub>:GUS*, *as2-163;RCOg-V;AtBP<sub>pro</sub>:GUS* and *RCOg-V;AtBP<sub>pro</sub>:GUS* plants from the F3 populations were used for GUS staining. The same method was applied to introduce *UBQ10<sub>pro</sub>:PM-Tdtomato*,<sup>58</sup> *DR5v2<sub>pro</sub>:Tdtomato*,<sup>37</sup> and *CYCB1;2<sub>pro</sub>:CYCB1;2-GUS*<sup>40</sup> (first named as *cyc1At::GUS*,<sup>40</sup> with the first ~150 amino acids fused with GUS) into *as1-151;RCOg-V* and *as2-163;RCOg-V* backgrounds.

### Quantitative PCR

For the qPCR experiment in Figures S1F and S1G, *as1-151;RCOg-V*, *as2-163;RCOg-V*, *as1-155;RCOg-V*, *as2-12;RCOg-V* and Col-0 plants were grown on soil under long-day conditions. The 8<sup>th</sup> young rosette leaves (4-5 mm length) from 20-day-old plants were dissected for RNA extraction. There were three biological replicates for each genotype, and each replicate included 10-12 leaves. For Figure S2C, *A. thaliana pML-Hyg-35S<sub>pro</sub>:Amikn126* and *pML-Hyg* transgenic plants were grown on ½ MS plates with 25µg/ml hygromycin under long-day conditions. 2-week-old seedlings without roots were harvested for RNA extraction. There were three biological replicates for each genotype, and each replicate included more than 12 seedlings. The total RNA was extracted by Qiagen RNeasy Plant Mini Kit, then reverse-transcribed by SuperScript VIL0 cDNA Synthesis Kit (Invitrogen) to generate the first-strand cDNA. Quantitative PCR was performed in QuantStudio 3 Real-Time PCR System (ThermoFisher) with Power SYBR Green PCR Master Mix (ThermoFisher). *AtUBQ10* was used to normalize and quantify the expression of target genes. The primers used are listed in Table S2. Relative expression was calculated by 2<sup>-ΔΔCT</sup>. qPCR results were plotted by R package ggplot2.<sup>62</sup>

### β -Glucuronidase (GUS) staining

The aerial part of plants was harvested and fixed in 90% acetone (v/v) for 30 min at room temperature. Then the samples were washed three times with GUS-staining buffer [50mM phosphate buffer pH7.2, 2mM K4Fe(CN)6, 2mM K3Fe(CN)6, 0.1% Triton X-100 (v/v), 10mM EDTA] and then incubated at 37°C with 1 mg/ml of 5-bromo-4-chloro-3-indolyl-β-D-glucuronic acid (X-gluc, Roth) in GUS-staining buffer. Samples were incubated for 10 hours (*AtBP<sub>pro</sub>:GUS* and *CYCB1;2<sub>pro</sub>:CYCB1;2-GUS*). After incubation, the staining buffer was removed, then 20%-50%-70% ethanol (v/v) was applied to clear the samples. GUS staining images were collected with a Nikon SMZ18 stereomicroscope and a Zeiss Axiophot light microscope.

### Confocal microscopy

A Leica SP8 upright confocal laser-scanning microscope was used for confocal imaging. Time-lapse images were captured with a long working-distance water immersion objective lens (20x/0.5, 40x/0.8, or 25x/0.95). The other confocal images were captured with these water-immersion objective lenses or a dry 10x/0.30 lens. Excitation was performed using an argon laser with 488 nm for GFP, 512 nm for VENUS, and a DPSS laser with 561 nm for Tdtomato/mCherry. Images were collected at 493-515 nm for GFP, 520-550 nm for VENUS, 580-620 nm for mCherry, 575-620 nm for Tdtomato, and 660-749 nm for chlorophyll auto-fluorescence. Images were

processed using Leica application suite X and Fiji<sup>59</sup> to generate maximum projections from representative confocal micrographs (Figures 3G–3I, S2I, and S2J).

### Time-lapse experiments and growth analysis

For each sample used in the time-lapse experiment, the cotyledons and older leaves were removed to expose the 8<sup>th</sup> ± 1 rosette leaves for imaging. The abaxial epidermis of the leaves was imaged at 24h intervals. Cell outlines were visualized by *UBQ10<sub>pro</sub>:PM-Tdtomato*. Confocal stacks for the time-lapse series were acquired at 512x512 or 1024x1024 resolution, at 400Hz speed, with 0.6–1.5 μm distance in Z-dimension depending on the leaf size. No line or frame average was used in order to minimize the imaging stress. Samples larger than the scanning area were imaged in parts and the stacks were stitched in MorphoGraphX (MGX) software.<sup>60,63</sup>

The cell lineage tracing and growth analysis were performed using MorphoGraphX. Raw images were processed using the standard pipeline to obtain cellular segmentation on a curved organ surface mesh (see the MorphoGraphX user guide<sup>64</sup> for details). Next, the cell lineages were determined for all time points to quantify the growth parameters (area extension, cell proliferation and growth anisotropy) and generate the heatmaps.<sup>60,63</sup> Area extension was computed as the relative growth of cell area between two time points.<sup>28</sup>

$$\text{area extension} = \frac{\text{cell area (timepoint 2)} - \text{cell area (timepoint 1)}}{\text{cell area (timepoint 1)}} \times 100\%$$

Here “cell area (timepoint 2)” refers to the clonal sector including all cells that were originated from a single cell at time point 1. Cell proliferation was computed as the number of cells at time point 2 that were originated from a single cell at time point 1.<sup>28</sup> Growth anisotropy was computed as the ratio of the maximal and minimal principal growth directions.<sup>60</sup>

For reverse cell fate mapping, the corresponding cell lineages through multiple days were computed by linking the parent relations between successive days, thus allowing the tracing of leaf structures, i.e. rachises and petiolules, back to the original cell populations (similar to the analysis in Kierzkowski et al.<sup>16</sup>). For the analysis shown in Figures 4C, 4D, S6B, and S6C, cells at the base of the first time point were manually selected as the origin to compute a distance coordinate system for the cells in the leaf. Based on those coordinates, we determined the basal 25% of the leaf cells (Figure 4C) which were used for the analysis (similar to the analysis in Zhang et al.<sup>37</sup>). Moreover, we divided the leaf into midrib and leaf blade cells based on geometrical cell features at the last time point. For further analysis of growth directions (Figures 5E and 5F), we used the organ coordinates to compute the proximal-distal axis in leaves. The medial-lateral axis was defined as the orthogonal direction to the proximal-distal axis. The Principal Directions of Growth were computed and their proximal-distal and medial-lateral components were determined using the previously defined organ axes. Similarly, in Figures 5I and 5J we computed the proximal-distal and medial-lateral axes of protrusions, by creating a distance field defined by a manually selected cell at the protrusion tip. To analyze sinus cells in Figures 5C–5F, we used 6 DAL leaves to manually select a region consisting of five layers of cells in the sinus region between the protrusions, and excluded cells that were part of the younger protrusion. The basal protrusion cells in Figures 5G–5J were selected as basal 50% of all protrusion cells. For plot and statistical analysis, all cellular data of geometry and growth were exported from MorphoGraphX and subsequently analyzed using R<sup>61</sup> and ggplot2.<sup>62</sup> For Figures 5L and 5M, the published time-lapse data of *C. hirsuta* wild type<sup>16</sup> were reanalyzed to understand the growth anisotropy in rachises. To create Video S1 we used MorphoGraphX to export frames of morphed segmented meshes of the different genotypes with their interpolated heatmaps. Those frames were used to create the animation using the open-source software FFmpeg.

### Leaf shape and protrusion morphospace analysis

Plant leaves were flattened onto white paper using transparent adhesive films, then digitally scanned with 800dpi resolution to obtain the silhouettes. Leaf shape space principle component analysis (Figure 2B) was performed using the software Leaf Interrogator as described previously<sup>37</sup> with two modifications. First, there were 9 out of 20 *as1-151;RCOg-V* leaf silhouettes bearing leaflets only on either side (5 right, 4 left). Because this type of leaf shape variance is not related to leaf complexity, those 4 leaf silhouettes bearing leaflets on the right side were flipped to make sure all 9 silhouettes showed left-side leaflets. Second, scale normalization was obtained by scaling each contour by the inverse of the centroid size to guarantee scale invariance. The protrusion morphospace plots with triangle approximation (Figures 1J, 5K, S4A, and S4B) were based on previously reported analysis,<sup>16</sup> with the protrusion triangles (length and basal width) measured from the silhouettes or confocal images by the software Fiji.<sup>59</sup> The R package ggplot2<sup>62</sup> was applied to draw the box/point/ribbon plots and the protrusion morphospaces.

### Leaf epidermal impressions

Leaf epidermal impressions were taken from the abaxial surface of rosette leaves by using transparent nail polish (Maybelline New York). The nail polish was applied to the leaf surface. After 10 minutes, the dried polish layer was peeled by fine forceps, mounted on slides, and imaged using the differential interference contrast (DIC) mode of a Zeiss Axiophot light microscope.

### Plasmid construction and plant transformation

For *pML-Hyg-35S<sub>pro</sub>:Amikn126*, the artificial miRNA was designed based on the web microRNA designer WMD3 (<http://wmd3.weigelworld.org>). Two amiRNAs were tandemly linked to knock down *AtBP* (TAATACGACGTATAAACTCCC) and *AtKNAT2/AtKNAT6*

(TTATATCGCAGTAGGTTTCCC). The amiRNA scaffold was synthesized (Genscript Biotech) and inserted into *pBJ36-35S-OCS* by *XhoI/XbaI*. The cassettes were cut by *NotI* and inserted into *pML-Hyg*. For *pML-Hyg-AtAS2<sub>pro</sub>:AtBP-mCherry*, The *AtAS2* promoter (4465bp) was amplified from *A. thaliana* genomic DNA with *Sall/Xmal* in the primers by Phusion high-fidelity DNA polymerase (NEB). *AtBP-mCherry* (the coding sequences of *AtBP* fused with *mCherry*) was synthesized with *Xmal/XbaI* in the flanking regions (Genscript Biotech). The *AtAS2* promoter and *AtBP-mCherry* sequences were ligated into to *pBJ36* by *Sall/Xmal/XbaI*, then the whole cassettes were cut by *NotI* and inserted into *pML-Hyg*.

Constructs were transformed into *A. thaliana* using *Agrobacterium* GV3103 and by the floral dip method.<sup>65</sup> *pML-Hyg-35S<sub>pro</sub>:Amikn126* and *pML-Hyg* (empty vector) were transformed into *as1/2;RCOg-V* plants. *pML-Hyg-AtAS2<sub>pro</sub>:AtBP-mCherry* was transformed into *RCOg-V* plants. T1 seeds were germinated on ½ MS plates with 25 mg/L hygromycin (Roth) for screening. Hygromycin-resistant T1 seedlings were transplanted on soil to grow and phenotype. T2 plants were screened by hygromycin again to confirm the transgene and phenotype. qPCR was used to validate the function of *35S<sub>pro</sub>:Amikn126* (Figure S2C). Fluorescent signal was examined to validate the expression of *AtAS2<sub>pro</sub>:AtBP-mCherry* (Figure S2I and S2J). To phenotype *AtAS2<sub>pro</sub>:AtBP-mCherry* plants in Col-0 background, four independent *AtAS2<sub>pro</sub>:AtBP-mCherry;RCOg-V* lines were crossed to Col-0. The F2 generations were genotyped to exclude presence of *RCOg-V* in the genome.

### QUANTIFICATION AND STATISTICAL ANALYSIS

Statistical analysis was performed by R.<sup>61</sup> The numbers of samples and replicates that were analyzed have been indicated in the figure legends. The significance threshold used was  $p < 0.05$ . For Figures 2C, S1F, and S1G, one-way ANOVA combined with Tukey HSD tests was applied to test the differences among genotypes. For Figures 4D, 5D–5F, 5H–5J, and S6C, nested ANOVA and post-hoc comparison (Tukey) were applied to test the significance of differences, with genotype treated as a fixed effect and sample treated as a random effect. For Figures S2C and S6B, Welch two-sample t-test was applied. For Figures 5K and S4A, A likelihood ratio test was applied to compare the protrusion growth (the estimated slopes of lineage models). The test was based on the principle that, if there was no difference in the relation between length and base size for each genotype, then there would be no significant improvement for a model allowing the slope for each genotype to be different over a model that had a single slope for all genotypes.